

February 24, 2022

# Recent Developments in the Study of Deconfinement in Nucleus-Nucleus Collisions

M. Gazdzicki,<sup>1,2</sup> M.I. Gorenstein,<sup>3,4</sup> and P. Seyboth<sup>5,2</sup>

<sup>1</sup>*Goethe-University, Frankfurt, Germany*

<sup>2</sup>*Jan Kochanowski University, Kielce, Poland*

<sup>3</sup>*Bogolyubov Institute for Theoretical Physics, Kiev, Ukraine*

<sup>4</sup>*Frankfurt Institute for Advanced Studies, Frankfurt, Germany*

<sup>5</sup>*Max-Planck-Institut fuer Physik, Munich, Germany*

## Abstract

Deconfinement refers to the creation of a state of quasi-free quarks and gluons in strongly interacting matter. Model predictions and experimental evidence for the onset of deconfinement in nucleus-nucleus collisions were discussed in our first review on this subject. These results motivated further experimental and theoretical studies. This review addresses two subjects. First, a summary of the past, present and future experimental programmes related to discovery and study of properties of the onset of deconfinement are presented. Second, recent progress is reviewed on analysis methods and preliminary experimental results for new strongly intensive fluctuation measures are discussed, which are relevant for current and future studies of the onset of deconfinement and searches for the critical point of strongly interacting matter.

PACS numbers: 12.40.-y, 12.40.Ee

Keywords: Onset of deconfinement, nucleus-nucleus collisions, event-by-event fluctuations

## Contents

<b>I. Introduction</b>	<b>3</b>
<b>II. Review of experimental programmes</b>	<b>5</b>
A. First Pb-beam Programme at the CERN SPS - Observation of the Phase Transition in Nucleus–Nucleus Collisions	5
1. A Brief History of Ideas	5
2. A Brief History of Experiments	6
B. Present Second Generation Heavy–Ion Experiments	9
1. System Size and Energy Scan Programme at the CERN SPS - Study of Properties of the Phase Transition in Nucleus–Nucleus Collisions	9
2. Beam Energy Scan Programme at the BNL RHIC	11
3. LHC: Collider and Fixed Target Experiments on Hot QGP	14
C. Future Experimental Programmes	16
1. NICA: Collider Studies of the Properties of the Mixed Phase	16
2. FAIR: Fixed Target Studies of High Baryon Density Matter	17
<b>III. Progress on Analysis Methods of Event-by-Event Fluctuations</b>	<b>18</b>
A. Fluctuations in the Number of Participants	19
B. Strongly Intensive Quantities $\Delta$ and $\Sigma$	25
1. $\Delta$ and $\Sigma$ in the Independent Particle Model	27
2. $\Delta$ and $\Sigma$ in the Multiple Independent Source (MIS) model	31
3. $\Delta$ and $\Sigma$ Evaluated in Specific Models	34
4. First Experimental Results on $\Delta[P_T, N]$ and $\Sigma[P_T, N]$ in p+p and Pb+Pb Collisions	38
C. Fluctuation Studies with Incomplete Particle Identification	40
1. The Identity Method	40
2. First Results on Fluctuations Based on the Identity Method	45
<b>IV. Closing Remarks</b>	<b>49</b>
<b>References</b>	<b>50</b>

## I. INTRODUCTION

Ordinary hadron matter is believed to be composed of hadrons in which constituent quarks and gluons are confined. At high temperature and/or pressure hadrons will be so densely packed that they are expected to dissolve into a new phase of quasi-free quarks and gluons, the quark-gluon-plasma (QGP). Theoretical considerations lead to a phase diagram of strongly interacting matter as shown schematically in Fig. 1 [1]. The existence region of hadrons at low temperature  $T$  and high baryochemical potential  $\mu_B$  is believed to be separated from the QGP at high  $T$  by a first order phase boundary, which ends with decreasing  $\mu_B$  in a critical point and then turns into a crossover transition. Experimentally the phase diagram has been explored by studying the final states produced in nucleus-nucleus collisions. The location of the freeze-out points is obtained from fitting the measured ratios of particle yields to a statistical model with  $T$  and  $\mu_B$  as parameters [2]. It was found that with increasing collision energy  $T$  increases and  $\mu_B$  decreases along a smooth freeze-out curve [3].

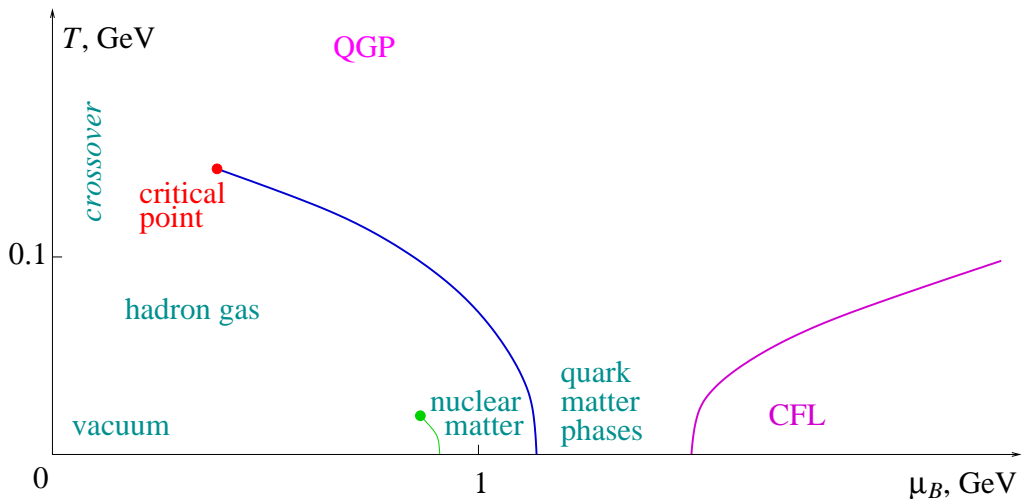


Figure 1: Semi-quantitative sketch of the phase diagram of strongly interacting matter [1].

Experimental searches for QGP signals started at the Super Proton Synchrotron (SPS) of the European Organization for Nuclear Research (CERN) and the Alternating Gradient Synchrotron (AGS) of Brookhaven National Laboratory (BNL) in the mid 1980s. Today they are pursued also at much higher collision energies at the Large Hadron Collider (LHC) at CERN and at the Relativistic Heavy Ion Collider (RHIC) at BNL.

Most probably the QGP is formed at the early stage of heavy ion collisions already at the top SPS energy [4]. Unambiguous evidence of the QGP state is, however, nearly impossible to obtain since quantitative predictions of proposed QGP signals [5–7] from the theory of strong interactions are difficult. For this reason the NA49 Collaboration at the CERN SPS has searched over the past years for signs of the onset of QGP creation in the energy dependence of hadron production properties. This search was motivated by a statistical model [8] showing that the onset of deconfinement should lead to rapid changes of the energy dependence of numerous experimentally detectable properties of the collisions, all appearing in a common energy domain. The predicted features were observed [9, 10] and dedicated experiments now continue detailed studies in the energy region of the onset of deconfinement. Model predictions and experimental evidence for the onset of deconfinement were discussed in our first review on this subject [11].

The present review addresses two subjects which have seen significant advances over the last years.

First, present and future experimental programmes related to the discovery and study of the onset of deconfinement are summarized. We start with a historical sketch of the NA49 beam energy scan with central Pb+Pb collisions which led to the discovery of the onset of deconfinement. Next we review the experimental programmes which are presently under way: NA61/SHINE at the CERN SPS, BES at the BNL RHIC and Heavy Ions at the CERN LHC. We close the chapter by summarizing the well advanced work on two new large facilities, MPD at JINR NICA and CBM at FAIR SIS-100.

Second, we review recent progress on analysis methods of event-by-event fluctuations in nucleus-nucleus collisions, which are relevant for the current and future studies of the onset of deconfinement and the search for the critical point. The experimental and theoretical progress in studies of event-by-event fluctuations seems to have the highest priority in the field of heavy ion collisions. After more than 40 years of experimental efforts we have now rich and relatively well understood experimental data on single particle spectra in Pb+Pb and p+p interactions from several GeV to several TeV. But, mostly due to the incomplete acceptance of detectors and not well developed data analysis tools, results on event-by-event fluctuations are not yet mature. High-quality and systematic measurements of event-by-event fluctuations are needed mostly for two reasons:

- to test statistical and dynamical models - the simplest tests at the level of fluctuations are still missing and
- to study properties of the phase transition, in particular properties of the transition at the onset of deconfinement and search for the critical point of strongly interacting matter.

## II. REVIEW OF EXPERIMENTAL PROGRAMMES

In this section the present and future experimental programmes related to the study of properties of the onset of deconfinement are reviewed. First, however, the history of the programme which led to the discovery of the onset of deconfinement, namely the beam energy scan programme with central Pb+Pb collisions at the CERN SPS is briefly recalled.

### A. First Pb-beam Programme at the CERN SPS - Observation of the Phase Transition in Nucleus–Nucleus Collisions

During the period 1999-2002 experimental data on Pb+Pb collisions were recorded by several experiments (NA49, NA45, NA57, NA50 and NA60) first at the top SPS energy of  $158A$  GeV. The primary aim of this program was to find evidence for the QGP in these reactions. Results were consistent with the signals expected for the production of this new state of matter [5] but not unique. This led to the extension of the program to lower beam energies ( $20A$ ,  $30A$ ,  $40A$ ,  $80A$  GeV) in order to search for a clear onset of deconfinement which was predicted to be at the low SPS energies. Only NA49 participated in the full energy scan. The history and the basic results of the SPS energy scan programme are reviewed in the following.

#### 1. *A Brief History of Ideas*

In the mid 90s numerous results on collisions of light nuclei at the BNL AGS (beams of Si at  $14.6A$  GeV) and the CERN SPS (beams of O and S at  $200A$  GeV) were obtained. The experiments with heavy nuclei (AGS: Au+Au at  $11.6A$  GeV, SPS: Pb+Pb at  $158A$  GeV) were just starting. This was the time when the first look at the energy dependence of hadron production in nucleus–nucleus (A+A) collisions at high energies became possible. Compilations,

on pion production [12] and on strangeness production [13] resulted in a clear conclusion: the energy dependence of hadron multiplicities measured in A+A collisions and p+p interactions are very different. Furthermore the data on A+A collisions suggested that there is a significant change in the energy dependence of pion and strangeness yields which is located between the top AGS and SPS energies. Based on the statistical approach to strong interactions [14, 15] it was conjectured [16–18] that the change is related to the onset of deconfinement during the early stage of the A+A collisions. Soon after, following this hypothesis, a quantitative model was developed, the Statistical Model of the Early Stage (SMES) [8]. It assumes creation of the early-stage matter according to the principle of maximum entropy. Depending on the beam energy  $E$  the matter is in the confined ( $E < 30A$  GeV), mixed ( $30A < E < 60A$  GeV) or deconfined ( $E > 60A$  GeV) phases. The phase transition is assumed to be of the first order.

## 2. *A Brief History of Experiments*

Based on these ideas the NA49 Collaboration proposed in 1997 to study hadron production in Pb+Pb collisions at  $30A$  GeV [19]. At this energy the SMES predicted a sharp maximum of the strangeness to pion ratio as a characteristic signal of the onset of deconfinement. Following this request a  $40A$  GeV Pb-beam was delivered to NA49 in 1998 as a test. The 5 weeks long run at  $40A$  GeV took place in 1999<sup>1</sup>. Data were registered by NA49, NA45, NA50 and NA57. The success of this first run at low SPS energy and the exciting preliminary results shown by NA49 justified a continuation of the program. In 2000 a beam at  $80A$  GeV was delivered for 5 days to NA49 and NA45 and the energy scan program was completed in 2002. Results of the analysis suggested that there is a significant change in the energy dependence of pion and strangeness yields which is located between the top AGS and SPS energies. Based on the SMES [8] it was concluded [11] that the change is related to the onset of deconfinement at the early stage of A+A collisions.

Results from this programme were published [20–29] and mostly concern the energy dependence of hadron production in central Pb+Pb collisions at  $20A$ ,  $30A$ ,  $40A$ ,  $80A$  and  $158A$  GeV.

---

<sup>1</sup> This program was started with  $40A$  GeV instead of the originally requested  $30A$  GeV due to technical SPS reasons.

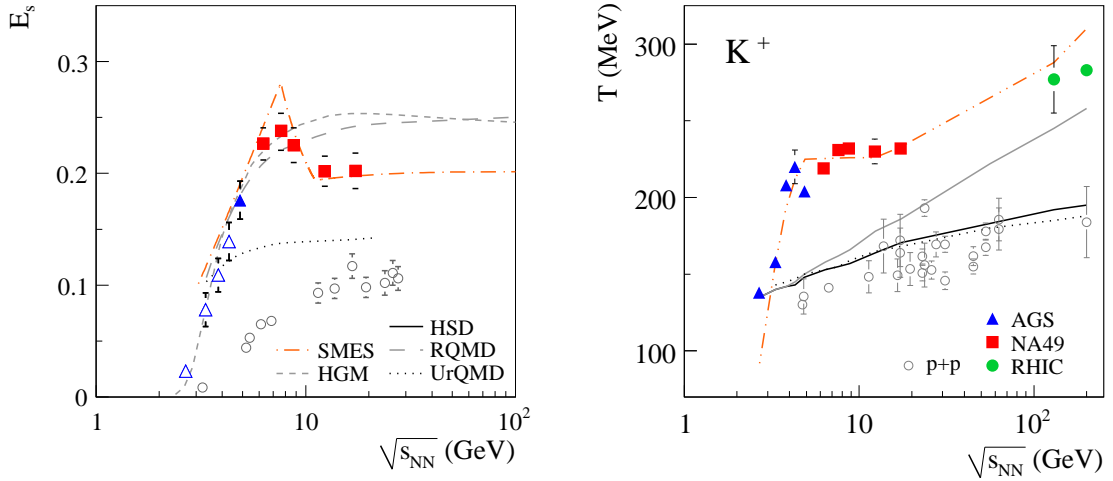


Figure 2: Dependence of hadron production properties in central Pb+Pb (Au+Au) collisions (closed symbols) and p+p interactions (open symbols) on the nucleon-nucleon cms energy  $\sqrt{s_{NN}}$ . Left: relative strangeness production as measured by the ratio  $E_S = (\langle\Lambda\rangle) + \langle K + \bar{K} \rangle / \langle\pi\rangle$ . Right: inverse slope parameter  $T$  of the transverse mass spectra of  $K^+$  mesons. The results for Pb+Pb (Au+Au) reactions are compared with various models. For details see text.

Key results and their comparison with models are summarized in Fig. 2 for the energy dependence of relative strangeness production measured by the  $E_S$  ratio (*left*) and the inverse slope parameter  $T$  of the transverse mass spectra of  $K^+$  mesons (*right*). The rapid changes in the SPS energy range for central Pb+Pb collisions (solid squares) suggest the onset of new physics in heavy ion collisions at low SPS energies. The energy dependence of the same observables measured in p+p interactions (open symbols in Fig. 2) is very different from that measured in central Pb+Pb (Au+Au) collisions and does not show any anomalies.

Relative strangeness production rises to a peak and then drops to a plateau at a value predicted for deconfined matter [8]. The energy dependence of the  $T$  parameter shows the step behaviour typically expected for a  $1^{st}$  order phase transition [30] and the resulting softness of the equation of state in the mixed-phase regime [31].

Models which do not assume the deconfinement phase transition (HGM [32], RQMD [33], UrQMD [34] and HSD [35, 36]) fail to describe the data. The introduction of a  $1^{st}$  order phase transition at low SPS energies (SMES [8] and hydrodynamic evolution of the fireball [37–39])

allow to describe the measured structures in the energy dependence of  $T$  and  $E_S$  (see dash-dotted curves in Fig. 2).

There are attempts to explain the results on nucleus-nucleus collisions by (model dependent) extrapolations of the results from proton-nucleus interactions [40, 41]. As detailed enough p+A data exist only at the top AGS and SPS energies the extrapolations are possible only at these two energies and thus there are no predictions of the energy dependence of the quantities relevant for the onset of deconfinement (see Fig. 2). The underlying models are based on the assumption that particle yields in the projectile hemisphere are due to production from excited projectile nucleon(s). This assumption is, however, in contradiction to the recent results at RHIC [42] and SPS [43] energies which clearly demonstrate a strong mixing of the projectile and target nucleon contributions in the projectile hemisphere. Furthermore, qualitative statements on similarity or differences between p+A and A+A reactions may be strongly misleading because of a trivial kinematic reason. The center of mass system in p+A interactions moves toward the target nucleus A with increasing A, whereas its position is A-independent for A+A collisions. For illustration several typical examples are considered. The baryon longitudinal momentum distribution in A+A collisions gets narrower with increasing A and, of course, it remains symmetric in the center of mass system. In p+A collisions it shrinks in the proton hemisphere and broadens in the target hemisphere (for example see slide 5 in Ref. [40]). Thus a naive comparison would lead to the conclusion that A+A collisions are qualitatively similar to p+A interactions if the proton hemisphere is considered, or that they are qualitatively different if the target hemisphere is examined. One encounters a similar difficulty when discussing the A-dependence of particle ratios in a limited acceptance. For instance the kaon to pion ratio is independent of A in p+A interactions if the total yields are considered [44], it is however strongly A-dependent in a limited acceptance (e.g. see slides 10 and 11 in Ref. [40]). Recent string-hadronic models [33–36] take all trivial kinematic effects into account and parameterize reasonably well p+p and p+A results. Nevertheless they fail to reproduce the A+A data (see e.g. Fig. 2).



## B. Present Second Generation Heavy-Ion Experiments

### 1. *System Size and Energy Scan Programme at the CERN SPS - Study of Properties of the Phase Transition in Nucleus–Nucleus Collisions*

Already in 2003 it was realized [45] that further progress in understanding effects related to the onset of deconfinement can only be achieved by a new comprehensive study of hadron production in proton-proton, proton-nucleus and nucleus-nucleus collisions.

The two most important open questions are:

- what is the nature of the transition from the anomalous energy dependence measured in central Pb+Pb collisions at SPS energies to the smooth dependence measured in p+p interactions ?
- is it possible to observe the predicted signals of the onset of deconfinement in fluctuations [46, 47] and anisotropic flow [48, 49] ?

These questions motivated the present ion programme at the CERN SPS devoted to an extensive system size and energy scan. Moreover, the programme received further urgency from the possibility to discover the critical point of strongly interacting matter. The programme was proposed to CERN in November 2006 [50]. Based on this proposal, pilot data taking took place in September 2007. The first physics data with hadron beams were recorded in 2009 and with ion beams (secondary  $^7\text{Be}$  beams) in 2011.

NA61/SHINE [51] is the only experiment which records data within this programme. It is a multi-purpose facility to study hadron production in hadron-proton, hadron-nucleus and nucleus-nucleus collisions at the CERN SPS. NA61/SHINE has greatly profited from the long development of the CERN proton and ion sources, the accelerator chain, as well as the H2 beam-line of the CERN North Area. The latter has recently been modified to also serve as a fragment separator as needed to produce the Be beams for NA61/SHINE. Numerous components of the NA61/SHINE set-up were inherited from its predecessors, in particular, the last one, the NA49 experiment. Important upgrades increased the data taking rate by a factor 10 and significantly improved the capability for defining the centrality of the collisions.

The status and plans of data taking of NA61/SHINE are summarized in Fig. 3. First results

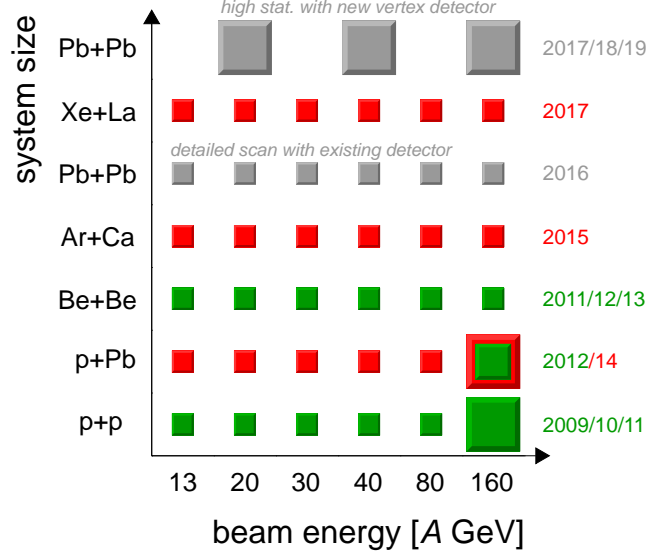


Figure 3: The NA61/SHINE data taking schedule for the ion program and its proposed extension for the period 2016–2019 (in gray). The proposed energy scan with Pb+Pb collisions in 2016 is needed to significantly decrease statistical and systematic uncertainties of results on Pb+Pb collisions by superseding the NA49 results with new NA61/SHINE measurements. The high statistics runs for Pb+Pb collisions with the new vertex detector are suggested in the period 2017-2019. They will allow for precise measurements of multi-strange hyperons and for first measurements of the open charm production at the top SPS energies.

were already obtained for inclusive spectra and fluctuations of identified hadrons produced in p+p and  ${}^7\text{Be}+{}^9\text{Be}$  interactions [52].

Two possible extensions of the NA61/SHINE ion programme are proposed. First, a detailed energy scan with Pb+Pb collisions at beam energies of 13A, 19A, 30A, 40A, 75A, 150A GeV is planned for 2016. Within a single data-taking period (42 days) data at all energies can be recorded with a typical event statistics of about 10 times the one of the NA49 data. This, together with the important detector upgrades, will allow to significantly decrease statistical and systematic uncertainties of results on Pb+Pb collisions by superseding the NA49 results with new NA61/SHINE measurements. Second, high-statistics measurements of Pb+Pb collisions at 19A, 40A and 150A GeV/c beam energy are foreseen in the period 2017–2019 after upgrading the NA61/SHINE apparatus by adding a vertex detector. They should allow to determine the

energy dependence of rare processes, in particular, production of  $D^0$  mesons at the top SPS energies and multi-strange hyperons in the full SPS energy range.

Moreover measurements of di-muon production in the SPS energy range is considered by two proto-collaborations, NA60+ and CHIC [53].

## 2. Beam Energy Scan Programme at the BNL RHIC

In parallel to the NA61/SHINE programme the Beam Energy Scan (BES) Programme at the BNL RHIC was proposed [54]. Both programmes were motivated by the NA49 results on the onset of deconfinement and the possibility to observe the critical point (CP) of strongly interacting matter.

The present goal of the BES programme related to the onset of deconfinement is summarized in ref. [55]. The aim is to find whether (and where in collision energy) the key QGP signatures observed at the top RHIC energy will turn off. This may indicate below which energy the system stays in the hadron gas phase. The disappearance of a single signature would not be enough to claim the onset of deconfinement, because there are other phenomena not related to deconfinement which may cause a similar effect. However, the modification or disappearance of several signatures simultaneously would definitely provide a compelling case. The particular observables identified as the essential drivers of this part of the run are: constituent quark number scaling (NCQ), hadron suppression in central collisions characterized by the ratio  $R_{cp}$  between particle yields in peripheral and central collisions, untriggered pair correlations in the space of pair separation in azimuth and pseudo-rapidity, local parity violation in strong interactions and strong fluctuations as possible indications of the CP.

In 2010 and 2011 RHIC completed phase I of the BES programme recording data on Au+Au collisions at nucleon-nucleon c.m.s. collision energies  $\sqrt{s_{NN}} = 7.7, 11.5, 19, 27$  and  $39$  GeV. This is complemented by the data collected earlier at higher energies ( $62, 130$  and  $200$  GeV). The phase II of the BES [56] is foreseen for 2017-2018 after the RHIC and STAR detector upgrades. Data taking on Au+Au collisions with the STAR detector is planned in the collider mode and, parasitically, in the fixed target mode down to a collision energy of  $3$  GeV.

Results from the BES phase I [57] show that elliptic flow, quantified by  $v_2$ , scales according to the NCQ down to the lowest energy (see Fig. 4). Flow develops at the very early stage of the

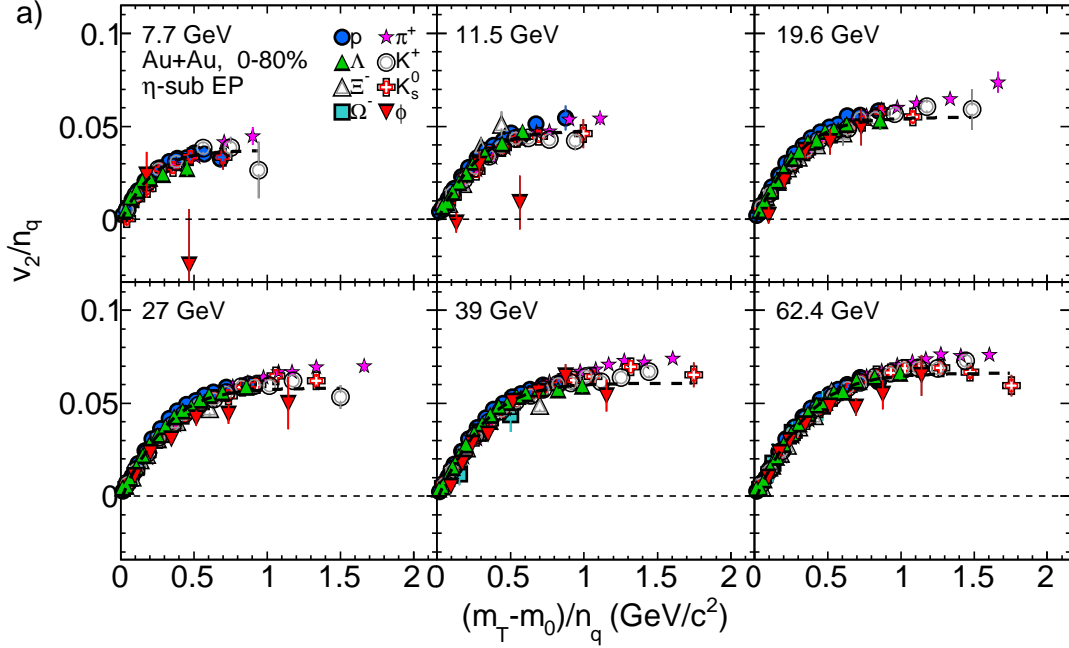


Figure 4: The Number-of-Constituent Quark (NCQ) scaled elliptic flow,  $v_2/n_q$  versus  $(m_T - m_0)/n_q$ , for 0–80% central Au+Au collisions for selected particles and the various collision energies of the RHIC beam energy scan [57]. Here  $n_q$  denotes the number of constituent quarks in particle of type  $q$  and  $m_0$  and  $m_T$  the particle rest mass and transverse mass, respectively. The dashed lines show the results of a parameterisation fitted simultaneously to all particles except the pions.

reaction from the anisotropic pressure in the almond-shaped interaction region of non-central collisions. If the fireball is in a partonic state at this stage, flow is thought to be imparted to the constituents from which the observed hadrons are coalescing. This picture would lead to the observed NCQ scaling.

The ratio  $R_{cp}$  is widely used to characterize the energy loss of partons in the fireball matter. When the fireball is in the QGP phase the high gluon density is expected to lead to strong attenuation of the parton energy (jet quenching) and a resulting suppression of particle spectra at large transverse momenta  $p_T$ . Preliminary results on  $R_{cp}$  [58] (see Fig. 5) show a monotonic evolution with collision energy from enhancement at low energy (the Cronin effect) to suppression at high energy. Thus, the BES did not observe any threshold-like changes, in addition to

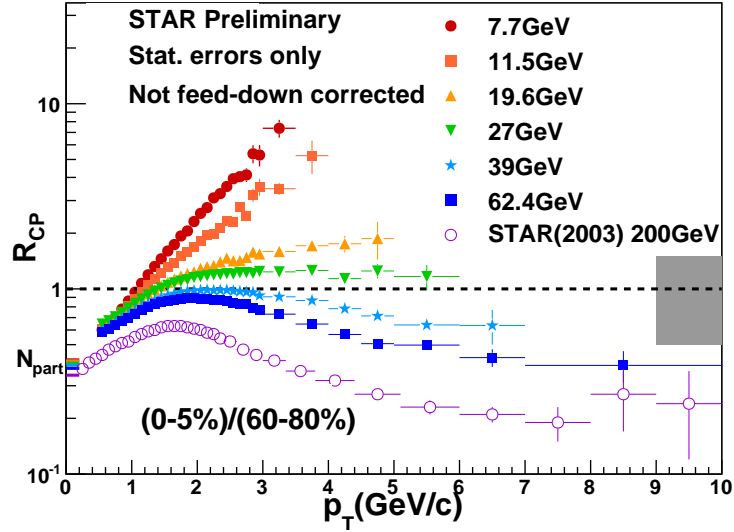


Figure 5: The STAR preliminary results of the energy dependence of charged particles  $R_{CP}$  [58]. The error bars on points reflect statistical errors. The systematic error (gray box) is independent of energy and  $p_T$ , and combines error on  $N_{coll}$  scaling and on the yields due to the background.

those reported by NA49.

It was pointed out in Ref. [59] that fluctuations of the net-proton multiplicities are a suitable experimental observable of the effects of a CP. The higher moments of the multiplicity distribution are expected to be especially sensitive [60–62]. The STAR collaboration recently published results from the BES programme [63] for the variance  $\sigma$ , the skewness  $S$  and the kurtosis  $\kappa$  of the net-proton multiplicity in Au+Au collisions (see Fig. 6). Measurements of  $\kappa\sigma$  and  $S\sigma$  are compared to the hadron-resonance gas model, the UrQMD model, and the reference Skellam distribution (the distribution of a random variable defined as the difference of two independent random variables following Poisson distributions). The values of  $S\sigma$  are close to the Skellam distribution and there appears to be a decreasing trend with decreasing energy for  $\kappa\sigma$  which is qualitatively reproduced by the UrQMD model. No firm conclusion with regard to the CP can be drawn at present, but more precise data are expected from the future BES II program.

It is important to note that the preliminary results from BES confirm the NA49 measurements relevant for the evidence for the onset of deconfinement. This will be illustrated in the following section.

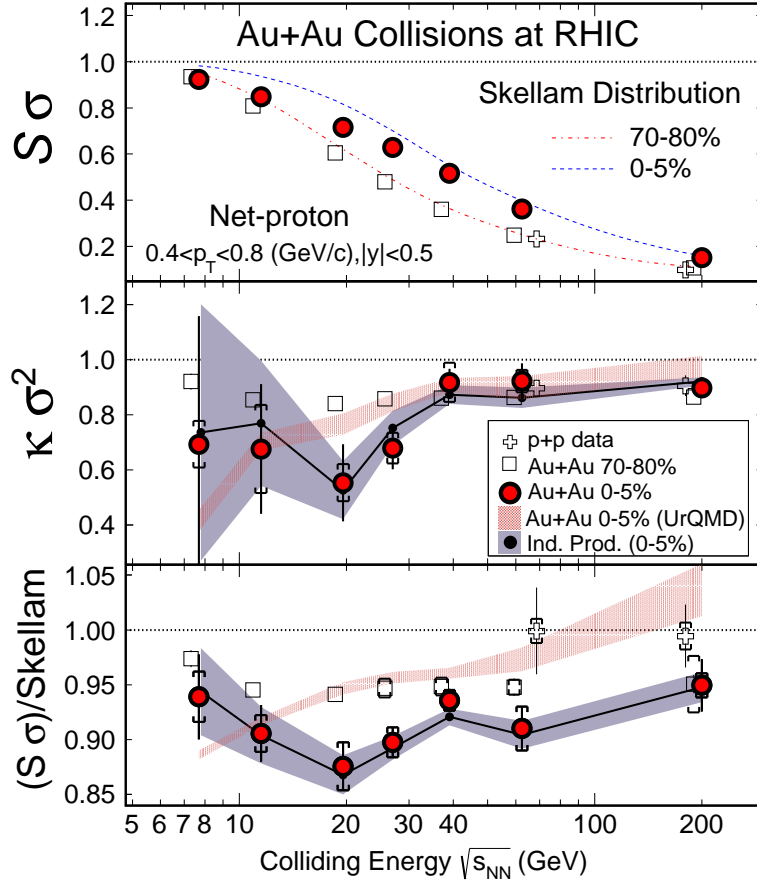


Figure 6: Collision energy and centrality dependence of the products of the variance  $\sigma$ , the skewness  $S$  and the kurtosis  $\kappa$  of the net-proton multiplicity distribution in Au+Au collisions [63]. The experimental results are compared to the reference Skellam distribution as well as predictions of the UrQMD model. For a hadron-resonance gas  $\kappa\sigma$  and  $S\sigma/\text{Skellam}$  are close to unity.

### 3. LHC: Collider and Fixed Target Experiments on Hot QGP

In 2011 first results on central Pb+Pb collisions at the LHC were released. These data were recorded at  $\sqrt{s_{NN}} = 2.76$  TeV, a nucleon-nucleon cms energy which is approximately 360 times higher than that of the onset of deconfinement. Nevertheless, these results are important to verify the interpretation of the NA49 results.

The updated plots on the energy dependence of hadron production properties are shown in Fig. 7 [64]. They include LHC data and results from the RHIC BES programme. The RHIC results [65, 66] confirm the NA49 measurements at the onset energies. The LHC data [67, 68]

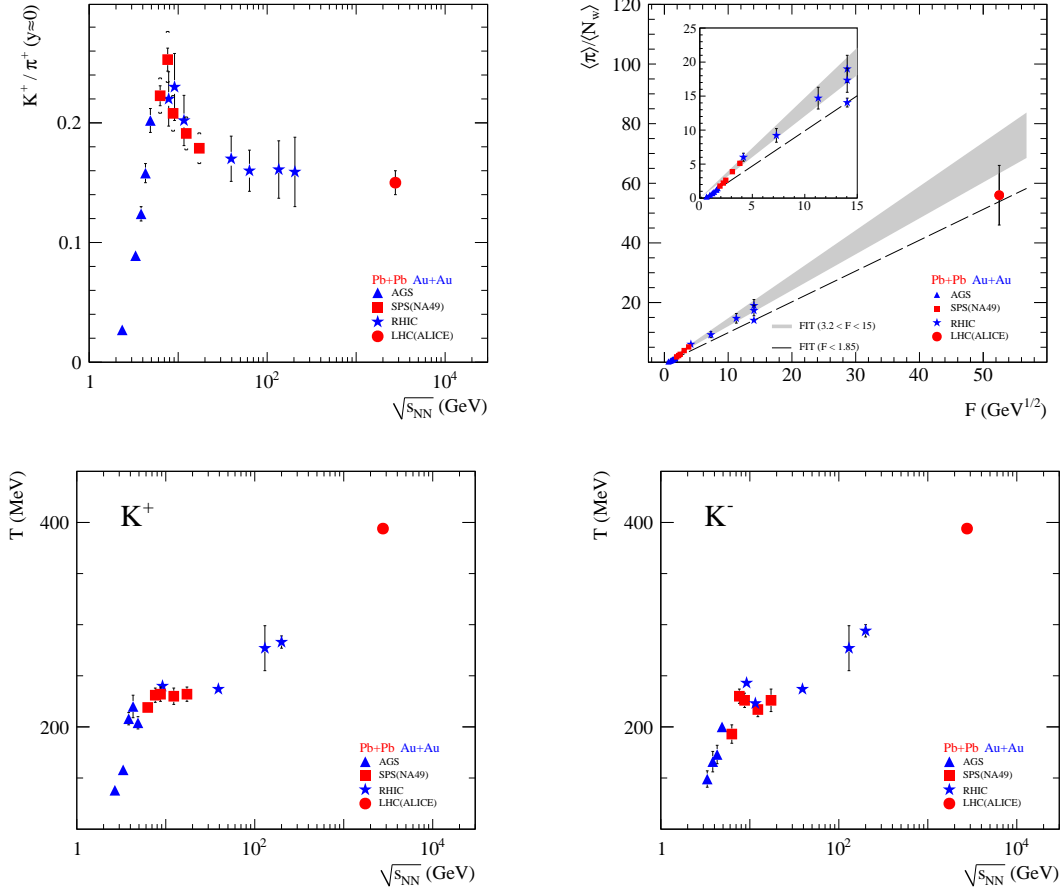


Figure 7: Heating curves of strongly interacting matter, status mid-2010. Hadron production properties (see Ref. [11] for details) are plotted as a function of collision energy ( $F \approx \sqrt{s_{NN}}$ ) for central Pb+Pb (Au+Au) collisions: *top-left* – the  $\langle K^+ \rangle / \langle \pi^+ \rangle$  ratio, *top-right* – the mean pion multiplicity per participant nucleon, bottom – the inverse slope parameter of the transverse mass spectra of  $K^+$  (*left*) and  $K^-$  (*right*) mesons. The new LHC and RHIC data are included in the *horn* (*top-left*), *kink* (*top-right*) and *step* (*bottom*) plots. The  $K^+/\pi^+$  ratio is measured by ALICE [67] and STAR [65] at mid-rapidity only and thus the *horn* plot is shown here for the mid-rapidity data. The observed changes of the energy dependence for central Pb+Pb (Au+Au) collisions are related to: decrease of the mass of strangeness carriers and the ratio of strange to non-strange degrees of freedom (*horn*: top-left plot), increase of entropy production (*kink*: top-right plot), weakening of transverse (*step*: bottom plots) expansion at the onset of deconfinement.

demonstrate that the energy dependence of hadron production properties shows rapid changes only at the low SPS energies. A smooth evolution is observed between the top SPS (17.2 GeV) and the current LHC (2.76 TeV) energies. This agrees with the interpretation of the NA49 structures as due to the onset of deconfinement. Above the onset energy only a smooth change of the quark-gluon plasma properties with increasing collision energy is expected. Thus currently there seems to be no strong physics motivation for measurements in the gap between the top RHIC and LHC energies.

A possibility to use proton and ion beams extracted from the LHC for future fixed target experiments is discussed since several years [69]. This would allow to extend the collision energy range of fixed target experiments up to about 70 GeV per nucleon–nucleon pair. This extension may be important in the search for the critical point of strongly interacting matter, if the current NA61/SHINE programme did not lead to its discovery at the SPS energies.

### C. Future Experimental Programmes

MPD [70] at NICA together with CBM [71] at SIS-100/300 belong to the third generation of experiments planned to study A+A collisions at energies of the CERN SPS.

#### 1. NICA: Collider Studies of the Properties of the Mixed Phase

Exploration of the transition between the confined and deconfined phases of strongly interacting matter is the top priority of the NICA programme [72].

The first round of NICA experiments intends to concentrate [73] on a variety of diagnostic observables that have already been employed in experimental programmes at SPS and RHIC (the beam energy scans); these are based on general considerations about phase changes and the associated different degrees of freedom. The MPD detector at NICA will be optimized for the study of fluctuations and correlations of bulk event properties and a primary goal will be to measure the excitation functions and the dependence of fluctuations and correlations on centrality and system size.

The observables include event-by-event fluctuations of multiplicity and transverse momentum of charged particles and identified particles (p, K,  $\pi$ ) as well as the corresponding joint



distributions. Correlation studies address long-range angular correlations like the transverse Fourier components  $v_1$  and  $v_2$  of identified particles (p, K,  $\pi$ ,  $\Lambda$ ), their antiparticles, and light clusters, as well as three-body correlations which are the basis for studying the chiral magnetic effect. Short-range two-particle correlations will be employed to measure the size and internal dynamics of the freeze-out stage. Particular care will be taken to provide as large as possible coverage in rapidity and transverse momentum. Measurements are planned as a function of collision energy for the following systems:

- p+p collisions,
- d+d collisions with a possibility to off-line select reactions with (p,p), (p,n), and (n,n) spectators,
- d+Pb collisions, and
- collisions of identical heavy nuclei, such as Pb+Pb.

For later also the study of collisions of identical nuclei of intermediate mass is envisaged. Clearly, when measuring correlations, the detector will simultaneously collect centrality-selected high-precision data on double differential spectra of identified hadrons. Thus, freeze-out conditions can be precisely established for collisions in the transition domain.

In a second stage of the experiment measurements of open-charm hadrons, di-leptons, and di-photons are also considered at NICA. The first data from the NICA programme are expected to come in 2017.

## 2. FAIR: Fixed Target Studies of High Baryon Density Matter

The Compressed Baryon Matter (CBM) experiment [71] is under construction at the GSI FAIR accelerator complex [74] which is expected to start delivering heavy ion beams from the SIS100 ring with energies up to  $11A$  GeV in 2018. The planned addition of SIS300 would extend the energy range to  $35A$  GeV after 2025. CBM will study strongly interacting matter from the region of the onset of deconfinement, where the highest initial stage baryon density is achieved [75], down to beam energies of  $2A$  GeV. Thus CBM will cover the energy domain of past AGS experiments and the low energy range of the SPS using a state-of-the-art detector.

The experiment will explore a region of the phase diagram where the CP and new forms of baryon-rich matter (e.g. quarkyonic matter) might be found.

CBM is designed to measure with unprecedented sensitivity spectra of hadrons, including multi-strange baryons and charmed mesons, as well as lepton pairs produced in p+p, p+A and A+A collisions. The research program focuses on the following observables [71]:

- Open and hidden charm production: measurements of yields and transport properties (anisotropic and radial flow) which are sensitive to the properties of the fireball medium (confined or partonic).
- Di-lepton pairs: study of in-medium properties of vector mesons via low-mass pairs (chiral restoration), search for virtual photon emission from a partonic phase in the intermediate mass region, study of the production properties of charmonia in the high-mass region (absorption in partonic matter).
- Yields and phase space distributions of hadrons (including multi-strange baryons): these are sensitive to the properties of the produced matter e.g. whether confined or deconfined, or possibly in an exotic state like quarkyonic matter.
- Hypernuclei: production expected via coalescence of  $\Lambda$  hyperons and nucleons providing information on hyperon-nucleon and hyperon-hyperon interactions which play an important role in neutron star models.
- Fluctuations and correlations: location and properties of the onset of deconfinement and search for the critical point.

The CBM programme can be expected to provide essential new knowledge on the properties of baryon-rich matter starting from 2018.

### III. PROGRESS ON ANALYSIS METHODS OF EVENT-BY-EVENT FLUCTUATIONS

The study of event-by-event (e-by-e) fluctuations in high-energy nucleus-nucleus collisions opens new possibilities to investigate properties of strongly interacting matter. (see, e.g.

Ref. [76] and references therein). Specific fluctuations can signal the onset of deconfinement when the collision energy becomes sufficiently high to create the QGP at the initial stage of A+A collision [46, 47]. By measuring the fluctuations, one may also observe effects caused by dynamical instabilities when the expanding system goes through the 1<sup>st</sup> order transition line between the QGP and the hadron-resonance gas [77, 78]. Furthermore, the critical point of strongly interacting matter may be signaled by a characteristic fluctuation pattern [79–83]. Therefore, e-by-e fluctuations are an important tool for the study of properties of the onset of deconfinement and the search for the CP of strongly interacting matter. However, mostly due to the incomplete acceptance of detectors and difficulties to control e-by-e the number of interacting nucleons as well as not well adapted data analysis tools, results on e-by-e fluctuations are not yet mature. Even the simplest tests of statistical and dynamical models at the level of fluctuations are still missing.

In this section progress in two areas related to the study of e-by-e fluctuations are reported. First, the role of fluctuations in the number of interacting nucleons is discussed and strongly intensive quantities are introduced. Second, a novel procedure, the identity method, is described for analyzing fluctuations of identified hadrons under typical experimental conditions of incomplete particle identification.

### A. Fluctuations in the Number of Participants

In each A+A collision only a fraction of all  $2A$  nucleons interact. These are called participant nucleons and are denoted as  $N_P^{proj}$  and  $N_P^{targ}$  for the projectile and target nuclei, respectively. The corresponding nucleons, which do not interact, are called the projectile and target spectators,  $N_S^{proj} = A - N_P^{proj}$  and  $N_S^{targ} = A - N_P^{targ}$ . The fluctuations in high energy A+A collisions are dominated by e-by-e variations of the impact parameter. However, even for a fixed impact parameter the participant numbers,  $N_P^{proj}$  and  $N_P^{targ}$ , fluctuate from event to event. This is due to the fluctuations of the initial states of the colliding nuclei and the probabilistic character of the interaction process. The fluctuations of  $N_P^{proj}$  and  $N_P^{targ}$  usually lead to a large and uninteresting background. In order to minimize its contribution fixed-target experiments select samples of collisions with a fixed number of projectile participants. This selection is achieved by the measurement of  $N_S^{proj}$  in each individual A+A collision by a calorimeter which covers

the projectile fragmentation domain. The advantage of this event selection is that it depends only on fluctuations of the initial state and is independent of the internal properties of the fireball created in the collisions. In collider experiments the number of spectators is impossible to measure because charged nuclear fragments follow the directions of the circulating beams. In these experiments events are typically selected using quantities derived from the produced hadrons, e.g. charged hadron multiplicity or transverse energy at mid-rapidity. This event selection has a significant disadvantage. Namely, it depends on the properties of the created fireball and may lead to a correlation between the quantity used for the event selection and the fluctuation quantities under study.

It was argued in Ref. [84] that any centrality selection in A+A collisions is equivalent to the geometrical selection via impact parameter  $b$ . Indeed, different centrality selection criteria result in approximately the same average values of physical quantities, e.g. average hadron multiplicities. However, they lead to rather different fluctuations of these quantities, e.g. different values of the scaled variances and correlations of hadron multiplicities. This was explicitly demonstrated in Ref. [85], where results for three different centrality selections – via impact parameter  $b$ , via the number of participants  $N_P$ , and via the charged particle multiplicities in the mid-rapidity window – were compared using the HSD transport approach to A+A collisions.

Even in fixed target experiments in which events with  $N_P^{proj} = const$  can be selected the number of target participants fluctuates considerably. Hence, an asymmetry between projectile and target participants is introduced, i.e.  $N_P^{proj}$  is constant by constraint, whereas  $N_P^{targ}$  fluctuates.

At fixed values of the numbers of participants  $N_P^{proj}$  and  $N_P^{targ}$  we introduce the probability  $W_i(N_i; N_P^{targ}, N_P^{proj})$  for producing  $N_i$  (the index  $i$  corresponds to the type of particle species, e.g.  $i = -, +, ch$ , i.e. negative, positive, all charged particles) final hadrons. At fixed  $N_P^{proj}$  the averaging procedure is defined as

$$\langle \dots \rangle \equiv \sum_{N_P^{targ} \geq 1}^A \sum_{N_i \geq 0} \dots W_P(N_P^{targ}; N_P^{proj}) W_i(N_i; N_P^{targ}, N_P^{proj}) , \quad (1)$$

where  $W(N_P^{targ}; N_P^{proj})$  is the probability for a given value of  $N_P^{targ}$  in a sample of events with fixed number of the projectile participants  $N_P^{proj}$ . The variance can be written as

$$Var(N_i) \equiv \langle N_i^2 \rangle - \langle N_i \rangle^2 = \omega_i^* \langle N_i \rangle + \omega_P n_i \langle N_i \rangle , \quad (2)$$

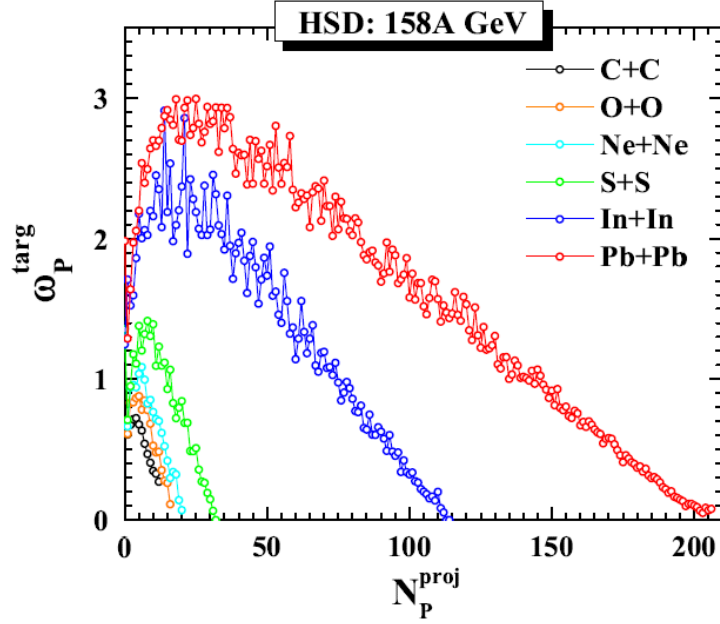


Figure 8: The scaled variance  $\omega_P^{targ}$  for the fluctuations of the number of target participants,  $N_P^{targ}$  as a function of the number of projectile participant,  $N_P^{proj}$  [86]. HSD simulations of  $\omega_P^{targ}$  are shown as a function of  $N_P^{proj}$  for different colliding nuclei (Pb+Pb, In+In, S+S, Ne+Ne, O+O and C+C) at  $E_{lab}=158$  AGeV.

where the scaled variance  $\omega_i^*$  corresponds to the fluctuations of  $N_i$  at fixed values of  $N_P^{proj}$  and  $N_P^{targ}$ ,  $n_i \equiv \langle N_i \rangle / \langle N_P \rangle$ , and  $N_P = N_P^{targ} + N_P^{proj}$  is the total number of participants. Eq. (2) is based on two assumptions: first, that  $\omega_i^*$  does not depend on  $N_P$ , and second, that the average multiplicities  $N_i$  are proportional to the number of participating nucleons. For the scaled variances,  $\omega_i$ , one finds

$$\omega_i \equiv \frac{Var(N_i)}{\langle N_i \rangle} = \omega_i^* + \omega_P n_i. \quad (3)$$

The average values are  $\langle N_P^{targ} \rangle \cong N_P^{proj}$ , thus,  $\langle N_P^{targ} \rangle \cong \langle N_P \rangle / 2$ . Therefore, the scaled variance  $\omega_P$  for the total number of participants in Eq. (3) equals to  $\omega_P = \omega_P^{targ} / 2$  as only half of the total number of participants fluctuate. The value of  $\omega_P^{targ}$  depends on  $N_P^{proj}$ , as shown in Fig. 8 by calculations using the HSD model for collisions of light, medium and large size nuclei at beam energy of 158A GeV [86].

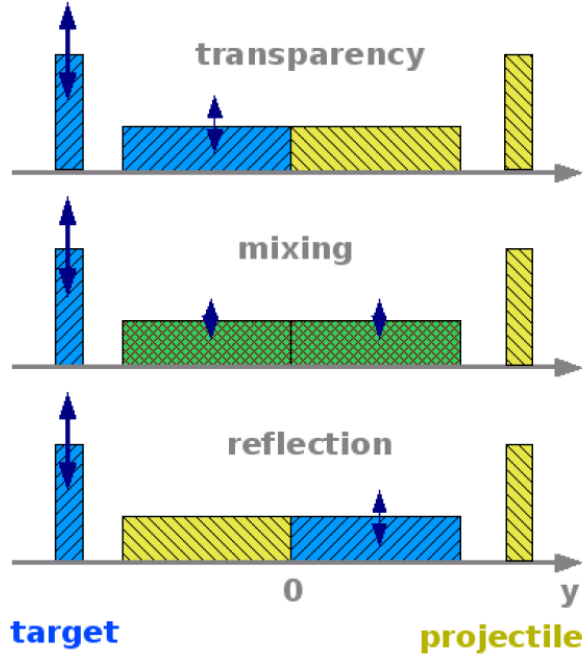


Figure 9: The schematic sketch of the rapidity distributions of the baryon number or the particle production sources (horizontal rectangles) in nucleus-nucleus collisions resulting from the transparency, mixing and reflection models. The spectator nucleons are indicated by the vertical rectangles. In the collisions with a fixed number of projectile spectators only matter related to the target shows significant fluctuations (vertical arrows). See Ref. [43] for more details.

Equation (3) corresponds to the so-called model of multiple independent sources (MIS). The model assumes that particles are produced by identical and independent sources. The numbers of sources are taken to be proportional to the number of projectile and target participant nucleons. The physical nature of the sources can be different, e.g. wounded nucleons [87], strings and resonances, or the fluid cells at chemical freeze-out in hydrodynamical models. Equation (3) gives the final multiplicity fluctuations as a sum of two terms: the fluctuations from one source,  $\omega_i^*$ , and the contribution due to the fluctuations of the number of sources,  $\omega_P n_i$ .

Models of hadron production in relativistic A+A collisions can be divided into three basic groups: transparency, mixing, and reflection models (see Ref. [43]). The first group assumes

that the final longitudinal flow of the hadron production sources related to projectile and target participants follows in the direction of the projectile and target, respectively. One calls this group transparency (T-)models. If the hadron production sources from projectile and target are mixed, these models are called mixing (M-)models. Finally, one may assume that the initial flows are reflected in the collision process. The projectile related matter then flows in the direction of the target and the target related matter flows in the direction of the projectile. This class of models is referred to as reflection (R-)models. The rapidity distributions resulting from the T-, M-, and R-models are sketched in Fig. 9.

An asymmetry between the projectile and target participants introduced by the experimental selection procedure in a fixed-target experiment can be used to distinguish between projectile related and target related final state flows of hadron production sources. The multiplicity fluctuations measured in the target momentum hemisphere clearly are larger than those measured in the projectile hemisphere in T-models. The opposite relation is predicted for R-models, whereas for M-models the fluctuations in the projectile and target hemispheres are expected to be the same. In collisions with a fixed number of  $N_P^{proj}$  and fluctuating number of  $N_P^{targ}$  the amount of mixing of projectile and target related matter in the final state of the collisions can be distinguished by an analysis of fluctuations.

As an illustrative example the fluctuations of the particle multiplicities in the projectile ( $y > 0$ ) and target ( $y < 0$ ) hemispheres are now considered within the transport models HSD and UrQMD (see Ref. [88]). As one can see from Fig. 8, the number of target participants,  $N_P^{targ}$ , fluctuates considerably in samples with  $N_P^{proj} = const$ . Because of this asymmetry between projectile and target participants the transport models give very different results for the particle number fluctuations (quantified by the scaled variance  $\omega$  of the multiplicity distribution) in the projectile and target hemispheres. As clearly seen from Fig. 10 the particle number fluctuations in the target hemisphere are much stronger than those in the projectile hemisphere. Note that there is also a strong  $N_P^{proj}$ -dependence of  $\omega_i$  in the target hemisphere, which is almost absent in the projectile hemisphere. Thus, the fluctuations of  $N_P^{targ}$  have a small influence on the final multiplicity fluctuations in the projectile hemisphere, but they contribute very strongly to those in the target hemisphere. These results demonstrate that the HSD and UrQMD transport models belong to the T-type. Note that they do not have enough mixing effects to explain the data in A+A collisions [43].

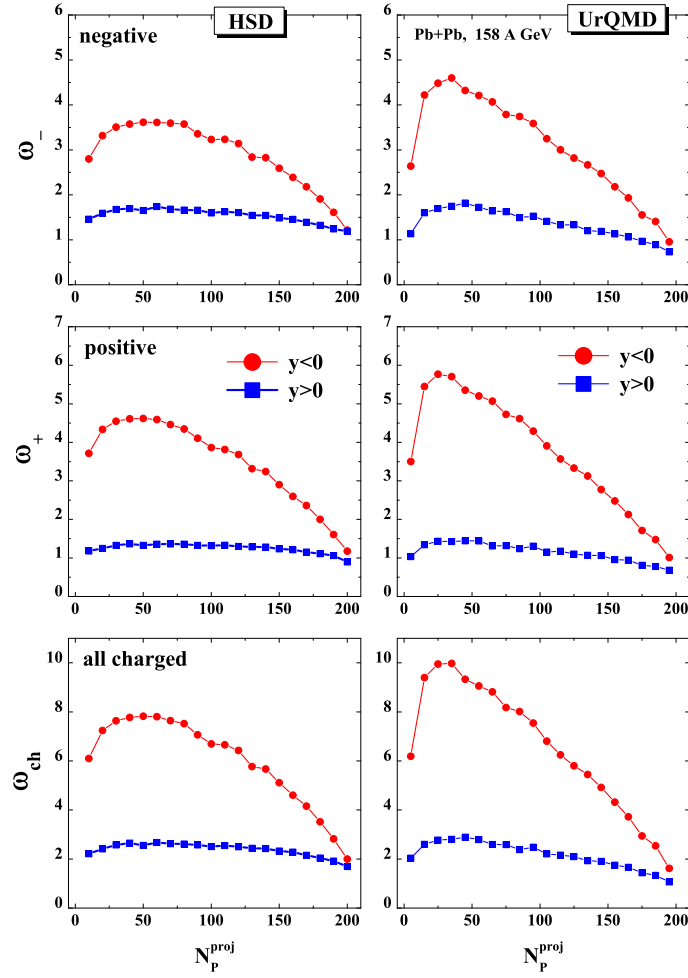


Figure 10: The scaled variance  $\omega_i$  of the multiplicity distribution for particles produced in the projectile (boxes) and target (circles) hemisphere in simulations of Pb+Pb collisions at beam energy of 158A GeV using the HSD (*left*) and UrQMD (*right*) models [88].

Some combination of the system size  $N_P$  and collision energy  $E_{lab}$  might move the chemical freeze-out point close to the QCD CP. One then expects an increase of multiplicity fluctuations with respect to their ‘background values’. Fig. 8 presents from the HSD model the scaled variance  $\omega_P^{targ}$  for C+C, O+O, Ne+Ne, S+S, In+In, and Pb+Pb collisions at 158 AGeV as a function of  $N_P^{proj}$ . Why does one need to study central collisions for ions of small and intermediate mass number  $A$  instead of peripheral Pb+Pb collisions in a search of the CP ?



Figure 8 explains this issue. At fixed  $N_P^{proj}$  the average total number of participants,  $N_P \equiv N_P^{proj} + N_P^{targ}$ , is equal to  $\langle N_P \rangle \cong 2N_P^{proj}$ , and, thus, it fluctuates as  $\omega_P = 0.5\omega_P^{targ}$ . Then, for example, the value of  $N_P^{proj} \cong 30$  corresponds to almost zero participant number fluctuations,  $\omega_P \cong 0$ , in S+S collisions while  $\omega_P$  becomes large and is close to 1 and 1.5 for In+In and Pb+Pb collisions of the same  $N_P^{proj}$ , respectively. Even if  $N_P^{proj}$  is fixed exactly, the sample of peripheral collision events in the heavy-ion case contains large fluctuations of the participant number: this would ‘mask’ the CP signals. As also seen from Fig. 8, the picture becomes actually more complicated if the atomic mass number  $A$  is small. In this case, the number of participants from the target fluctuates significantly even for the largest fixed value of  $N_P^{proj} = A$ .

## B. Strongly Intensive Quantities $\Delta$ and $\Sigma$

A significant increase of transverse momentum and multiplicity fluctuations is expected in the vicinity of the CP [79–81]. One can probe different regions of the phase diagram by varying the collision energy and size of colliding nuclei [89]. The possibility to observe signatures of the critical point inspired the energy and system size scan program of the NA61/SHINE Collaboration at the CERN SPS [90] and the BES program of the STAR and PHENIX Collaborations at the BNL RHIC [91]. In these studies one measures and then compares e-by-e fluctuations in collisions of different nuclei at different collision energies. The average sizes of the created physical systems and their fluctuations are expected to be rather different (see previous section III A). This strongly affects the observed fluctuations, i.e. the measured quantities would not describe the local physical properties of the system but rather reflect the system size fluctuations. For instance, A+A collisions with different centralities may produce a system with approximately the same local properties (e.g. the same temperature and baryonic chemical potential) but with the volume changing significantly from interaction to interaction. Note that in high energy collisions the average volume of created matter and its variations from collision to collision usually cannot be controlled experimentally. Therefore, a suitable choice of statistical tools for the study of e-by-e fluctuations is really important.

Intensive quantities are defined within the grand canonical ensemble of statistical mechanics. They depend on temperature and chemical potential(s), but they are independent of the system volume. Strongly intensive quantities introduced in Ref. [92] are, in addition, independent of

volume fluctuations. They are the appropriate measures for studies of e-by-e fluctuations in A+A collisions and can be defined from two, *extensive state quantities*  $A$  and  $B$ . Here, we call  $A$  and  $B$  *extensive* when the first moments of their distributions for the ensemble of possible states are proportional to volume. They are referred to as *state quantities* as they characterize the states of the considered system, e.g. final states of A+A collisions or micro-states of the grand canonical ensemble. For example,  $A$  and  $B$  may stand for multiplicities of kaons and pions, respectively, in a particular state.

There are two families of strongly intensive quantities which depend on the second and first moments of  $A$  and  $B$  and thus allow to study state-by-state fluctuations [92]:

$$\Delta[A, B] = \frac{1}{C_\Delta} \left[ \langle B \rangle \omega[A] - \langle A \rangle \omega[B] \right], \quad (4)$$

$$\Sigma[A, B] = \frac{1}{C_\Sigma} \left[ \langle B \rangle \omega[A] + \langle A \rangle \omega[B] - 2(\langle AB \rangle - \langle A \rangle \langle B \rangle) \right], \quad (5)$$

where

$$\omega[A] \equiv \frac{\langle A^2 \rangle - \langle A \rangle^2}{\langle A \rangle}, \quad \omega[B] \equiv \frac{\langle B^2 \rangle - \langle B \rangle^2}{\langle B \rangle}, \quad (6)$$

and averaging  $\langle \dots \rangle$  is performed over the ensemble of multi-particle states. The normalization factors  $C_\Delta$  and  $C_\Sigma$  are required to be proportional to the first moments of any extensive quantities.

In Ref. [93] a specific choice of the  $C_\Delta$  and  $C_\Sigma$  normalization factors was proposed. It makes the quantities  $\Delta[A, B]$  and  $\Sigma[A, B]$  dimensionless and leads to  $\Delta[A, B] = \Sigma[A, B] = 1$  in the independent particle model, as will be shown below.

From the definition of  $\Delta[A, B]$  and  $\Sigma[A, B]$  it follows that  $\Delta[A, B] = \Sigma[A, B] = 0$  in the case of absence of fluctuations of  $A$  and  $B$ , i.e., for  $\omega[A] = \omega[B] = \langle AB \rangle - \langle A \rangle \langle B \rangle = 0$ . Thus the proposed normalization of  $\Delta[A, B]$  and  $\Sigma[A, B]$  leads to a common scale on which the values of the fluctuation measures calculated for different state quantities  $A$  and  $B$  can be compared.

There is an important difference between the  $\Sigma[A, B]$  and  $\Delta[A, B]$  quantities. Namely, in order to calculate  $\Delta[A, B]$  one needs to measure only the first two moments:  $\langle A \rangle$ ,  $\langle B \rangle$  and  $\langle A^2 \rangle$ ,  $\langle B^2 \rangle$ . This can be done by independent measurements of the distributions  $P_A(A)$  and  $P_B(B)$ . The quantity  $\Sigma[A, B]$  includes the correlation term,  $\langle AB \rangle - \langle A \rangle \langle B \rangle$ , and thus requires, in addition, simultaneous measurements of  $A$  and  $B$  in order to obtain the joint distribution

$P_{AB}(A, B)$ . Under exchange of  $A$  and  $B$  the quantities  $\Sigma[A, B]$  and  $\Delta[A, B]$  have the property  $\Sigma[A, B] = \Sigma[B, A]$  and  $\Delta[A, B] = -\Delta[B, A]$ . Using the last relation one can always define  $\Delta \geq 0$  by exchanging the  $A$  and  $B$  quantities.

### 1. $\Delta$ and $\Sigma$ in the Independent Particle Model

The Independent Particle Model (IPM) assumes that:

- (i) the state quantities  $A$  and  $B$  can be expressed as

$$A = \alpha_1 + \alpha_2 + \dots + \alpha_N, \quad B = \beta_1 + \beta_2 + \dots + \beta_N, \quad (7)$$

where  $\alpha_j$  and  $\beta_j$  denote single particle contributions to  $A$  and  $B$ , respectively, and  $N$  is the number of particles;

- (ii) inter-particle correlations are absent, i.e. the probability of any multi-particle state is the product of probability distributions  $P(\alpha_j, \beta_j)$  of single-particle states, and these probability distributions are the same for all  $j = 1, \dots, N$  and independent of  $N$  :

$$P_N(\alpha_1, \beta_1, \alpha_2, \beta_2, \dots, \alpha_N, \beta_N) = \mathcal{P}(N) \times P(\alpha_1, \beta_1) \times P(\alpha_2, \beta_2) \times \dots \times P(\alpha_N, \beta_N), \quad (8)$$

where  $\mathcal{P}(N)$  is an arbitrary multiplicity distribution of particles.

It can be shown [93] that within the IPM the average values of the first and second moments of  $A$  and  $B$  are equal to:

$$\langle A \rangle = \bar{\alpha} \langle N \rangle, \quad \langle A^2 \rangle = \bar{\alpha^2} \langle N \rangle + \bar{\alpha}^2 [\langle N^2 \rangle - \langle N \rangle], \quad (9)$$

$$\langle B \rangle = \bar{\beta} \langle N \rangle, \quad \langle B^2 \rangle = \bar{\beta^2} \langle N \rangle + \bar{\beta}^2 [\langle N^2 \rangle - \langle N \rangle], \quad (10)$$

$$\langle AB \rangle = \bar{\alpha\beta} \langle N \rangle + \bar{\alpha} \cdot \bar{\beta} [\langle N^2 \rangle - \langle N \rangle]. \quad (11)$$

The values of  $\langle A \rangle$  and  $\langle B \rangle$  are proportional to the average number of particles  $\langle N \rangle$  and, thus, to the average size of the system. These quantities are extensive. The quantities  $\bar{\alpha}$ ,  $\bar{\beta}$  and  $\bar{\alpha^2}$ ,  $\bar{\beta^2}$ ,  $\bar{\alpha\beta}$  are the first and second moments of the single-particle distribution  $P(\alpha, \beta)$ . Within the IPM they are independent of  $\langle N \rangle$  and play the role of intensive quantities.

Using Eq. (9) the scaled variance  $\omega[A]$  which describes the state-by-state fluctuations of  $A$  can be expressed as:

$$\omega[A] \equiv \frac{\langle A^2 \rangle - \langle A \rangle^2}{\langle A \rangle} = \frac{\overline{\alpha^2} - \bar{\alpha}^2}{\bar{\alpha}} + \bar{\alpha} \frac{\langle N^2 \rangle - \langle N \rangle^2}{\langle N \rangle} \equiv \omega[\alpha] + \bar{\alpha} \omega[N], \quad (12)$$

where  $\omega[\alpha]$  is the scaled variance of the single-particle quantity  $\alpha$ , and  $\omega[N]$  is the scaled variance of  $N$ . A similar expression follows from Eq. (10) for the scaled variance  $\omega[B]$ . The scaled variances  $\omega[A]$  and  $\omega[B]$  depend on the fluctuations of the particle number via  $\omega[N]$ . Therefore,  $\omega[A]$  and  $\omega[B]$  are not strongly intensive quantities.

From Eqs. (9-11) one obtains expressions for  $\Delta[A, B]$  and  $\Sigma[A, B]$ , namely:

$$\Delta[A, B] = \frac{\langle N \rangle}{C_\Delta} \left[ \bar{\beta} \omega[\alpha] - \bar{\alpha} \omega[\beta] \right], \quad (13)$$

$$\Sigma[A, B] = \frac{\langle N \rangle}{C_\Sigma} \left[ \bar{\beta} \omega[\alpha] + \bar{\alpha} \omega[\beta] - 2 \left( \overline{\alpha \beta} - \bar{\alpha} \cdot \bar{\beta} \right) \right]. \quad (14)$$

Thus, the requirement that

$$\Delta[A, B] = \Sigma[A, B] = 1, \quad (15)$$

within the IPM leads to:

$$C_\Delta = \langle N \rangle \left[ \bar{\beta} \omega[\alpha] - \bar{\alpha} \omega[\beta] \right], \quad (16)$$

$$C_\Sigma = \langle N \rangle \left[ \bar{\beta} \omega[\alpha] + \bar{\alpha} \omega[\beta] - 2 \left( \overline{\alpha \beta} - \bar{\alpha} \cdot \bar{\beta} \right) \right]. \quad (17)$$

In the IPM the  $A$  and  $B$  quantities are expressed in terms of sums of the single particle variables,  $\alpha$  and  $\beta$ . Thus in order to calculate the normalization  $C_\Delta$  and  $C_\Sigma$  factors one has to measure the single particle quantities  $\alpha$  and  $\beta$ . However, this may not always be possible within a given experimental set-up. For example,  $A$  and  $B$  may be energies of particles measured by two calorimeters. Then one can study fluctuations in terms of  $\Delta[A, B]$  and  $\Sigma[A, B]$  but can not calculate the normalization factors which are proposed above.

For illustrative purposes we consider in more detail a specific pair of extensive variables: the transverse momentum  $A = P_T = p_T^{(1)} + \dots + p_T^{(N)}$ , where  $p_T^{(i)}$  is the absolute value of the  $i^{\text{th}}$  particle transverse momentum, and the number of particles  $B = N$ . To simplify notations we use  $X = P_T$  and  $x_i = p_T^{(i)}$ . Note that our consideration is also valid for other motional variables  $X$ , e.g. the system energy  $X = E = \epsilon_1 + \dots + \epsilon_N$ .

First, we consider the IPM which is used as a reference model to fix the normalization of the strongly intensive measures  $\Delta$  and  $\Sigma$ . The IPM assumes that  $A$ , the motional extensive variable, can be written as a sum of single particle terms

$$X = x_1 + x_2 + \dots + x_N , \quad (18)$$

and  $B = N$  is the number of particles. Inter-particle correlations are absent in the IPM, i.e. the probability of any multi-particle state is a product of probability distributions  $F(x_j)$  of single-particle variables  $x_j$ , and these probability distributions are the same for all  $j = 1, \dots, N$  and independent of the number of particles  $N$  :

$$F_N(x_1, x_2, \dots, x_N) = \mathcal{P}(N) \times F(x_1) F(x_2) \times \dots \times F(x_N) , \quad (19)$$

where  $\mathcal{P}(N)$  is an arbitrary multiplicity distribution of particles. The functions entering Eq. (19) satisfy the normalization conditions:

$$\sum_N \mathcal{P}(N) = 1 , \quad \int dx F(x) = 1 . \quad (20)$$

The averaging procedure for  $k^{\text{th}}$  moments of any multi-particle observable  $A$  reads:

$$\langle A^k \rangle = \sum_N \mathcal{P}(N) \int dx_1 dx_2 \dots dx_N F(x_1) F(x_2) \times \dots \times F(x_N) \left[ A(x_1, x_2, \dots, x_N) \right]^k . \quad (21)$$

For the first and second moments of  $X$  and  $N$  one obtains:

$$\langle X \rangle = \bar{x} \cdot \langle N \rangle , \quad \langle X^2 \rangle = \overline{x^2} \cdot \langle N \rangle + \bar{x}^2 \cdot [\langle N^2 \rangle - \langle N \rangle] , \quad \langle XN \rangle = \bar{x} \cdot \langle N^2 \rangle , \quad (22)$$

where

$$\langle N^k \rangle = \sum_N \mathcal{P}(N) N^k , \quad \overline{x^k} = \int dx F(x) x^k . \quad (23)$$

Note that the over-line denotes averaging over a single particle inclusive distribution, whereas  $\langle \dots \rangle$  represents event averaging over multi-particle states of the system, e.g. e-by-e averaging over hadrons detected in A+A collisions.

Using Eq. (22) one finds

$$\omega[X] \equiv \frac{\langle X^2 \rangle - \langle X \rangle^2}{\langle X \rangle} = \frac{\overline{x^2} - \bar{x}^2}{\bar{x}} + \bar{x} \cdot \frac{\langle N^2 \rangle - \langle N \rangle^2}{\langle N \rangle} \equiv \omega[x] + \bar{x} \cdot \omega[N] , \quad (24)$$

$$\langle XN \rangle - \langle X \rangle \langle N \rangle = \bar{x} \cdot [\langle N^2 \rangle - \langle N \rangle^2] \equiv \bar{x} \cdot \langle N \rangle \omega[N] , \quad (25)$$

and finally,

$$\Delta[X, N] = \frac{1}{C_\Delta} \left[ \langle N \rangle \omega[X] - \langle X \rangle \omega[N] \right] = \frac{\omega[x] \cdot \langle N \rangle}{C_\Delta}, \quad (26)$$

$$\Sigma[X, N] = \frac{1}{C_\Sigma} \left[ \langle N \rangle \omega[X] + \langle X \rangle \omega[N] - 2 \left( \langle X N \rangle - \langle X \rangle \langle N \rangle \right) \right] = \frac{\omega[x] \cdot \langle N \rangle}{C_\Sigma}. \quad (27)$$

The requirement that

$$\Delta[X, N] = \Sigma[X, N] = 1 \quad (28)$$

thus leads for the IPM to the normalization factors

$$C_\Delta = C_\Sigma = \omega[x] \cdot \langle N \rangle, \quad \omega[x] \equiv \frac{\overline{x^2} - \bar{x}^2}{\bar{x}}. \quad (29)$$

In the IPM the event quantity  $X$  can be expressed as a sum of single-particle quantities  $x_i$ , see Eq. (18). The single-particle quantities are needed to calculate the normalization factors  $C_\Delta$  and  $C_\Sigma$ . Note that the event quantity  $X$  can be measured directly without measurements of the  $x_i$  quantities.

As a next example let us consider multiplicity fluctuations. Here  $A$  and  $B$  will denote multiplicities of hadrons of types  $A$  and  $B$ , respectively (e.g. kaons and pions). Particle identities were introduced in Ref. [94] to study fluctuations between particle types, so-called “chemical” fluctuations. One defines the identities  $w_A^j$  and  $w_B^j$  as  $w_A^j = 1$  and  $w_B^j = 0$  if the  $j^{th}$  particle is of  $A$  type, and  $w_A^j = 0$  and  $w_B^j = 1$  if the  $j^{th}$  particle is of  $B$  type. For single-particle quantities  $\alpha \equiv w_A$  and  $\beta \equiv w_B$  one obtains:

$$\bar{\alpha} = \overline{\alpha^2} = \frac{\langle A \rangle}{\langle A + B \rangle}, \quad \bar{\beta} = \overline{\beta^2} = \frac{\langle B \rangle}{\langle A + B \rangle}, \quad \overline{\alpha \beta} = 0. \quad (30)$$

From Eq. (30) one then finds

$$\omega[\alpha] = \bar{\beta}, \quad \omega[\beta] = \bar{\alpha}, \quad \overline{\alpha \beta} - \bar{\alpha} \cdot \bar{\beta} = -\bar{\alpha} \cdot \bar{\beta}. \quad (31)$$

Using Eqs. (30) and (31) one obtains from Eqs. (16) and (17):

$$C_\Delta = \langle B \rangle - \langle A \rangle, \quad C_\Sigma = \langle A \rangle + \langle B \rangle. \quad (32)$$

As seen from Eq. (32) the normalization factors depend only on the first moments of extensive quantities  $A$  and  $B$ . In general, more information is needed to calculate  $C_\Delta$  and  $C_\Sigma$  when the

multiplicities  $A$  and  $B$  correspond to partly overlapping sets of particles, e.g.  $A = K^+ + K^-$  and  $B = H^-$ , where  $H^-$  means the number of all negatively charged hadrons.

The normalization factors (29) and (32) are suggested to be used for the calculation for  $\Delta$  and  $\Sigma$  both in theoretical models and for the analysis of experimental data (see Ref. [93] for further details of the normalization procedure).

As was noted in Ref. [92] the  $\Phi$  measure, introduced some time ago [95], belongs to the  $\Sigma$  family within the current classification scheme. The fluctuation measure  $\Phi$  was introduced for the study of transverse momentum fluctuations. In the general case, when  $A = X$  represents any motional variable and  $B = N$  is the particle multiplicity, one gets:

$$\Phi_X = \left[ \bar{x} \omega[x] \right]^{1/2} \left[ \sqrt{\Sigma[X, N]} - 1 \right]. \quad (33)$$

For the multiplicity fluctuations of hadrons belonging to non-overlapping types  $A$  and  $B$  the connection between the  $\Phi[A, B]$  and  $\Sigma[A, B]$  measures reads:

$$\Phi[A, B] = \frac{\sqrt{\langle A \rangle \langle B \rangle}}{\langle A \rangle + \langle B \rangle} \left[ \sqrt{\Sigma[A, B]} - 1 \right]. \quad (34)$$

The IPM plays an important role as the *reference model*. The deviations of real data from the IPM results Eq. (28) can be used to learn about the physical properties of the system. This resembles the situation in studies of particle multiplicity fluctuations. In this case, one uses the Poisson distribution  $P(N) = \exp(-\bar{N}) \bar{N}^N / N!$  with  $\omega[N] = 1$  as the reference model. The other reference value  $\omega[N] = 0$  corresponds to  $N = \text{const}$ , i.e. the absence of  $N$ -fluctuations. Values of  $\omega[N] > 1$  (or  $\omega[N] \gg 1$ ) correspond to “large” (or “very large”) fluctuations of  $N$ , and  $\omega[N] < 1$  (or  $\omega[N] \ll 1$ ) to “small” (or “very small”) fluctuations.

## 2. $\Delta$ and $\Sigma$ in the Multiple Independent Source (MIS) model

Next, we study the Multiple Independent Source (MIS) model for multi-particle production. In this model the number of sources,  $N_S$ , changes from event to event. The sources are statistically identical and independent of each other. A famous example of the MIS is the wounded nucleon model [87] for A+A collisions. Two fluctuating extensive quantities  $X$  and  $N$  can be expressed as

$$X = X_1 + X_2 + \dots + X_{N_S}, \quad N = n_1 + n_2 + \dots + n_{N_S}, \quad (35)$$

where  $n_j$  denotes the number of particles emitted from the  $j^{\text{th}}$  source ( $j = 1, \dots, N_S$ ), and  $X_j = x_1 + \dots + x_{n_j}$  is the contribution from the  $j^{\text{th}}$  source to the quantity  $X$ .

The over-line notations are used for the averages connected to a single source. The single-source quantities are independent of  $N_S$  and have the properties of intensive quantities. The single-source distribution  $F_S(X_S, n)$  is assumed to be statistically identical for all sources, thus, for all  $j = 1, \dots, N_S$  it follows:

$$\overline{X_j^k} \equiv \overline{X_S^k}, \quad \overline{n_j^k} \equiv \overline{n^k}, \quad \overline{X_j n_j} \equiv \overline{X_S n}, \quad (36)$$

where  $\overline{X_S^k}$ ,  $\overline{n^k}$ , and  $\overline{X_S n}$  (for  $k = 1, 2$ ) are the first and second moments of the distribution  $F_S(X_S, n)$  for a single source. The sources are assumed to be independent. This gives at  $i \neq j$ :

$$\overline{X_i X_j} \equiv \overline{X_S^2}, \quad \overline{n_i n_j} \equiv \overline{n^2}, \quad \overline{X_i n_j} \equiv \overline{X_S n}. \quad (37)$$

Using Eqs. (36) and (37) one finds for the event averages:

$$\langle X \rangle = \overline{X_S} \cdot \langle N_S \rangle, \quad \langle X^2 \rangle = \overline{X_S^2} \cdot \langle N_S \rangle + \overline{X_S^2} [\langle N_S^2 \rangle - \langle N_S \rangle], \quad (38)$$

$$\langle N \rangle = \overline{n} \langle N_S \rangle, \quad \langle N^2 \rangle = \overline{n^2} \cdot \langle N_S \rangle + \overline{n^2} \cdot [\langle N_S^2 \rangle - \langle N_S \rangle], \quad (39)$$

$$\langle X N \rangle = \overline{X_S n} \langle N_S \rangle + \overline{X_S} \overline{n} \cdot [\langle N_S^2 \rangle - \langle N_S \rangle]. \quad (40)$$

The probability distribution  $\mathcal{P}_S(N_S)$  of the number of sources is needed to calculate  $\langle N_S \rangle$  and  $\langle N_S^2 \rangle$  and, in general, it is unknown.

Using Eqs. (38-40) one obtains:

$$\omega[X] \equiv \frac{\langle X^2 \rangle - \langle X \rangle^2}{\langle X \rangle} = \frac{\overline{X_S^2} - \overline{X_S}^2}{\overline{X_S}} + \overline{X_S} \cdot \frac{\langle N_S^2 \rangle - \langle N_S \rangle^2}{\langle N_S \rangle} \equiv \omega[X_S] + \overline{X_S} \cdot \omega[N_S], \quad (41)$$

$$\omega[N] \equiv \frac{\langle N^2 \rangle - \langle N \rangle^2}{\langle N \rangle} = \frac{\overline{n^2} - \overline{n}^2}{\overline{n}} + \overline{n} \cdot \frac{\langle N_S^2 \rangle - \langle N_S \rangle^2}{\langle N_S \rangle} \equiv \omega[n] + \overline{n} \cdot \omega[N_S], \quad (42)$$

where  $\omega[X_S]$  and  $\omega[n]$  are the scaled variances for quantities  $X_S$  and  $n$  referring to a single source. The scaled variances  $\omega[X]$  and  $\omega[N]$  are independent of the average number of sources  $\langle N_S \rangle$ . Thus,  $\omega[X]$  and  $\omega[N]$  are intensive quantities. However, they depend on the fluctuations of the number of sources via  $\omega[N_S]$  and, therefore, they are not strongly intensive quantities.

From Eqs. (40-42) it follows:

$$\Delta[X, N] = \frac{1}{\omega[x]} \left[ \omega[X_S] - \overline{x} \cdot \omega[n] \right]. \quad (43)$$

$$\Sigma[X, N] = \frac{1}{\omega[x]} \left[ \omega[X_S] + \overline{x} \cdot \omega[n] - 2 \frac{\overline{X_S n} - \overline{x} \overline{n^2}}{\overline{n}} \right], \quad (44)$$



where the relations

$$\bar{x} = \frac{\overline{X_S}}{\bar{n}} = \frac{\langle X \rangle}{\langle N \rangle} , \quad (45)$$

and the normalization factors (29) were used.

Note that the terms with  $\langle N_S^2 \rangle$ , which are present in the expressions (38-40) for the second moments of  $X$  and  $N$ , are canceled out in the final expressions (43,44). From three second moments  $\langle X^2 \rangle$ ,  $\langle N^2 \rangle$ , and  $\langle X N \rangle$  just two linear combinations independent of  $\langle N_S^2 \rangle$  can be constructed. These are the strongly intensive quantities  $\Delta$  and  $\Sigma$ .

The IPM and MIS have a similar structure. The difference is that the number of particles  $N$  in the IPM is replaced by the number of sources  $N_S$  in the MIS. Each source can produce many particles, and the number of these particles varies from source to source and from event to event. Besides, the physical quantity  $X_S$  for particles emitted from the same source may include inter-particle correlations. Therefore, in general, the MIS does not satisfy the assumptions of the IPM. Nevertheless, a formal similarity between the two models can be exploited and gives the following rule of one to one correspondence: all results for the IPM can be found from the expressions obtained for the MIS, assuming artificially that each source always produces exactly one particle. In this case one finds

$$\bar{n} = 1 , \quad \omega[n] = 0 , \quad \omega[X_S] = \omega[x] , \quad \overline{X_S n} = \bar{x} , \quad (46)$$

and Eqs. (43-44) are transformed to Eq. (28).

If particles are independently emitted from a single source, one obtains

$$F_S(X_S, n) = \mathcal{P}_S(n) \times F_S(x_1) \times \cdots \times F_S(x_n) , \quad (47)$$

with the probability distributions  $F_S(x_i)$  which are the same for all  $i = 1, \dots, n$  and independent of the number of particles  $n$ . Similar to Eqs. (24) and (25) one then finds:

$$\omega[X_S] = \omega[x] + \bar{x} \cdot \omega[n] , \quad \overline{X_S n} - \overline{X_S} \bar{n} = \bar{x} \bar{n} \cdot \omega[n] , \quad (48)$$

and Eqs. (43) and (44) are again transformed to Eq. (28). Therefore, the MIS with independent particle emission from each source is equivalent to the IPM.

### 3. $\Delta$ and $\Sigma$ Evaluated in Specific Models

The most popular model which satisfies the IPM assumptions is the ideal Boltzmann multi-component gas in the grand canonical ensemble formulation, which we refer to as the IB-GCE. In the IB-GCE the probability of any microscopic state is equal to the product of probabilities of single-particle states. These probabilities are independent of particle multiplicity. Thus, the IB-GCE satisfies the assumption (8) of the IPM.

The IB-GCE predicts a specific form of the multiplicity distribution  $\mathcal{P}(N)$ , namely the Poisson distribution, and thus,  $\omega[N] = 1$ . Moreover, it also predicts the specific form of the single-particle probability in momentum space, namely the Boltzmann distribution:

$$f_B(\mathbf{p}) = C \exp\left(-\frac{\sqrt{\mathbf{p}^2 + m^2}}{T}\right), \quad (49)$$

where  $\mathbf{p}$  and  $m$  are particle momentum and mass, respectively,  $T$  is the system temperature, and  $C = \left[\int d^3p \exp[-\sqrt{p^2 + m^2}/T]\right]^{-1}$  is the normalization constant.

Note that by introducing quantum statistics one destroys the correspondence between the GCE and the IPM. This is because of (anti-)correlation between particles in the same quantum state for the (Fermi) Bose ideal gas. Moreover, correlations between particles are introduced if instead of resonances their decay products are considered. Note that it is necessary to include strong decays of resonances in order to compare the GCE predictions to experimental results.

The correspondence between the IB-GCE and the IPM remains valid even if the volume varies from micro-state to micro-state<sup>2</sup> but local properties of the system, i.e., temperature and chemical potentials are independent of the system volume. Let volume fluctuations be given by the probability density function  $F(V)$ . The averaging over all micro-states includes the averaging over the micro-states with fixed volume and the averaging over the volume fluctuations. The volume fluctuations broaden the  $\mathcal{P}(N)$  distribution and increase its scaled variance:

$$\omega[N] \equiv \frac{\langle N^2 \rangle - \langle N \rangle^2}{\langle N \rangle} = 1 + \frac{\langle N \rangle}{\langle V \rangle} \cdot \frac{\overline{V^2} - \overline{V}^2}{\overline{V}}, \quad (50)$$

where  $\overline{V^k} \equiv \int dV F(V) V^k$  for  $k = 1, 2$ . The first term on the right hand side of Eq. (50) corresponds to the particle number fluctuations in the IB-GCE at a fixed volume  $V$  (i.e., this

---

<sup>2</sup> Statistical ensembles with volume fluctuations were discussed in Ref. [96, 97]

is the scaled variance of the Poisson distribution), and the second term is the contribution due to the volume fluctuations. Equation (8) remains valid in this example, therefore, the IB-GCE with arbitrary volume fluctuations satisfies the IPM assumptions.

Frequently used by experimentalists is the Mixed Event Model employing a Monte Carlo procedure in order to create a sample of artificial events in which correlations and fluctuations present in the original ensemble of events are partly removed. The original and mixed events are analyzed in the same way and the corresponding results are compared in order to extract the magnitude of a signal of interest, which by construction should be present in the original events and absent in the mixed events. The mixed event procedure is in particular popular in studies of resonance production, particle correlations due to quantum statistics and event-by-event fluctuations, see for examples Ref. [98].

There are many variations of the Mixed Event Model. Here we describe the one which in the limit of infinite number of original and mixed events gives results identical to the IPM. The procedure to create a mixed event which corresponds to the given ensemble of original events consists of two steps, namely:

- (i) drawing a mixed event multiplicity,  $N$ , from the set of multiplicities of all original events;
- (ii) selecting randomly with replacement  $N$  particles for the mixed event from the set of all particles from all original events.

Then the steps one and two are repeated to create the next mixed event and the procedure is stopped when the desired number of mixed events is reached. In the limit of infinite number of original events, the probability to have two particles from the same original event in a single mixed event is zero and thus particles in the mixed events are uncorrelated. Therefore, in this limit the mixed event model satisfies the IPM assumptions. Note, for an infinite number of mixed events, the first moments of all extensive quantities and all single-particle distributions of the original and mixed events are identical.

The UrQMD model [34] was used in Ref. [93] to illustrate the study of the  $\Delta$  and  $\Sigma$  measures by numerical results. Figure 11 shows the collision energy dependence of these measures in the CERN SPS energy range. In this example,  $A = P_T$  is the total transverse momentum of negatively charged hadrons and  $B = H^-$  is their multiplicity. The UrQMD simulations were performed for inelastic p+p interactions and for the 7% most central Xe+La collisions. This

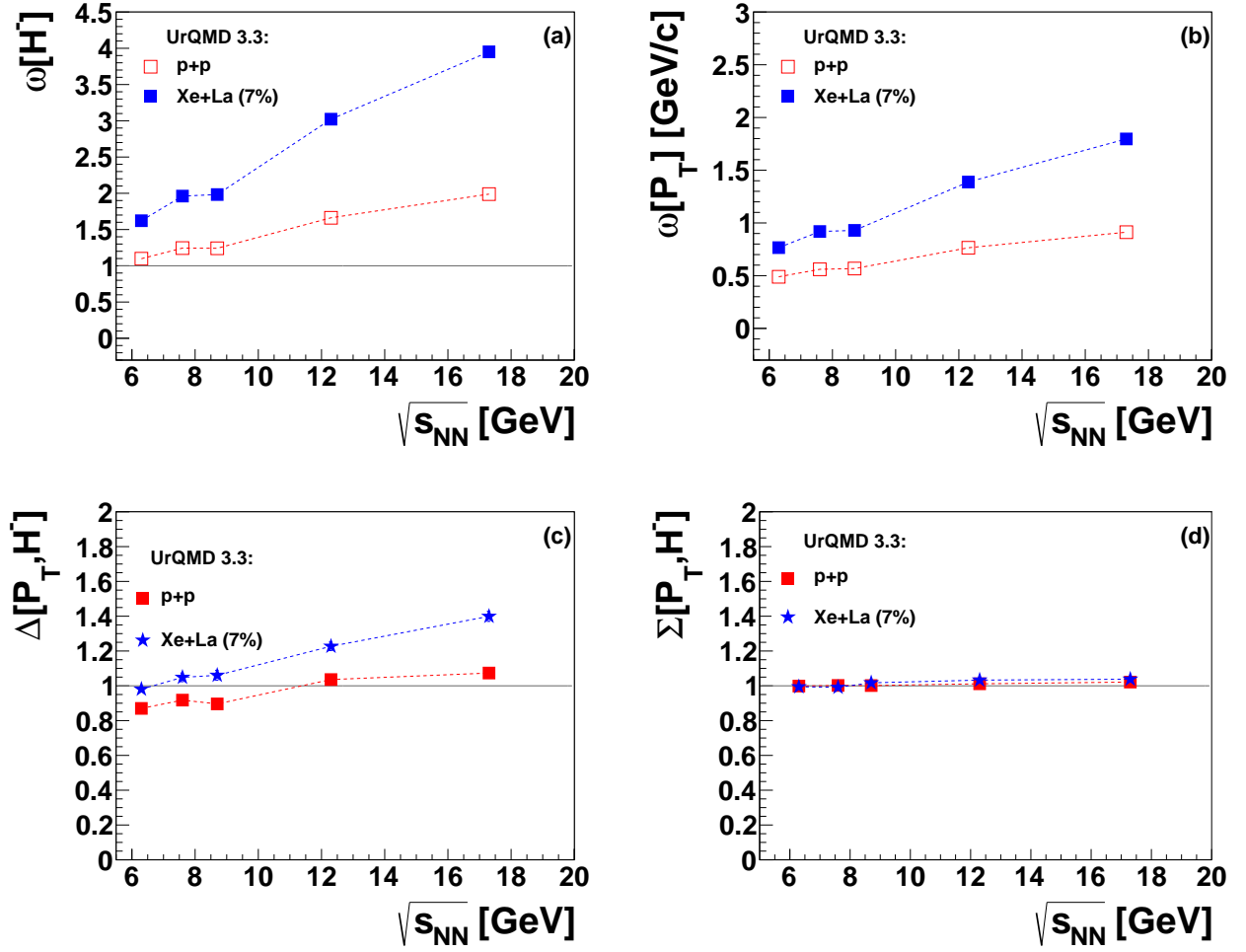


Figure 11: Fluctuation measures calculated within the UrQMD model for negatively charged hadrons produced in inelastic p+p interactions and the 7% most central Xe+La collisions as functions of collision energy in the CERN SPS energy range [93]. The top plots show intensive measures of fluctuations, namely the scaled variance of (a) the negatively charged hadron multiplicity,  $\omega[H^-]$ , and (b) the sum of magnitudes of their transverse momenta,  $\omega[P_T]$ . The bottom plots show the corresponding strongly intensive measures (c)  $\Delta[P_T, H^-]$  and (d)  $\Sigma[P_T, H^-]$ . Statistical uncertainties are smaller than the symbol size and were calculated using the subsample method.

choice of reactions is motivated by the experimental program of the NA61/SHINE Collaboration [99] at the CERN SPS. The top plots show intensive fluctuation measures, namely the scaled variance of the negatively charged particle multiplicity distribution,  $\omega[H^-]$ , and of the distribution of the sum of the magnitudes of their transverse momenta,  $\omega[P_T]$ . The bottom

plots show the corresponding strongly intensive measures  $\Delta[P_T, H^-]$  and  $\Sigma[P_T, H^-]$  normalized as proposed in Eq. (29).

The scaled variance of  $H^-$  and  $P_T$  is significantly larger in central Xe+La collisions than in p+p interactions. To a large extent this is due to fluctuations of the number of nucleons which interacted (wounded nucleons), see Ref. [100] for a detailed discussion of this issue. The advantages of the  $\Delta[P_T, H^-]$  and  $\Sigma[P_T, H^-]$  quantities are obvious from the results presented in the bottom plots. First, they are not directly sensitive to fluctuations of the collision geometry (the number of wounded nucleons) in contrast to the scaled variance. Second, they are dimensionless and expressed in units common for all energies and reactions. Due to the particular normalization proposed in Ref. [93], they assume the value one for the IPM and zero in the absence of event-by-event fluctuations. The UrQMD results for  $\Sigma[P_T, H^-]$  shown in Fig. 11 are close to unity both for p+p interactions and central Xe+La collisions. This is not the case for the  $\Delta[P_T, H^-]$  measure. One observes both a deviation from the IPM prediction  $\Delta[P_T, H^-] = 1$  and a difference between results for p+p interactions and central Xe+La collisions. Therefore, one concludes for the UrQMD model that the measure  $\Delta[P_T, H^-]$  is more sensitive to inter-particle correlations than the measure  $\Sigma[P_T, H^-]$ .

The strongly intensive fluctuation measures  $\Delta[P_T, N]$  and  $\Sigma[P_T, N]$  were recently studied in Ref. [101] for the ideal Bose and Fermi gas within the GCE. As already noted above, the GCE for the Boltzmann approximation satisfies the conditions of the IPM, i.e. Eq. (15) is valid in the IB-GCE. The following general relations were found [101]:

$$\Delta^{\text{Bose}}[P_T, N] < \Delta^{\text{Boltz}} = 1 < \Delta^{\text{Fermi}}[P_T, N] , \quad (51)$$

$$\Sigma^{\text{Fermi}}[P_T, N] < \Sigma^{\text{Boltz}} = 1 < \Sigma^{\text{Bose}}[P_T, N] , \quad (52)$$

i.e. the Bose statistics makes  $\Delta[P_T, N]$  smaller and  $\Sigma[P_T, N]$  larger than unity, whereas the Fermi statistics works in the opposite way. The Bose statistics of pions appears to be the main source of quantum statistics effects in a hadron gas with a temperature typical for the hadron system created in A+A collisions. It gives about 20% decrease of  $\Delta[P_T, N]$  and 10% increase of  $\Sigma[P_T, N]$ , at  $T \cong 150$  MeV with respect to the IPM results (15). The Fermi statistics of protons modifies insignificantly  $\Delta[P_T, N]$  and  $\Sigma[P_T, N]$  for typical values of  $T$  and  $\mu_B$ . Note that UrQMD takes into account several sources of fluctuations and correlations, e.g. the exact conservation laws and resonance decays. On the other hand, it does not include the effects of

Bose and Fermi statistics.

Other examples of Monte Carlo simulations and analytical model results for  $\Delta[P_T, N]$  and  $\Sigma[P_T, N]$  were presented in Refs. [102, 103].

#### 4. First Experimental Results on $\Delta[P_T, N]$ and $\Sigma[P_T, N]$ in $p+p$ and $Pb+Pb$ Collisions

Fluctuations of the average transverse momentum of charged particles have been investigated by the NA49 experiment for some time [21] employing the strongly intensive measure  $\Phi_{P_T}$  proposed in Ref. [95]. Published results for the energy dependence of  $\Phi_{P_T}$  in central  $Pb+Pb$  collisions are shown in Fig. 12 versus the baryochemical potential  $\mu_B$ . Also plotted for comparison are preliminary results of NA61/SHINE from inelastic  $p+p$  interactions. Curves show predictions [104, 105] for a critical point located at  $\mu_B = 360$  MeV [106]. Clearly there is no evidence for the expected maximum of fluctuations.

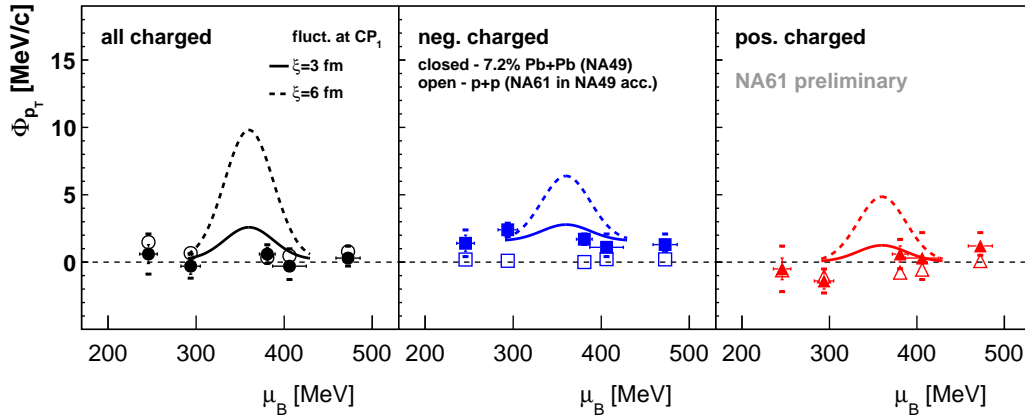


Figure 12: Fluctuation measure  $\Phi_{P_T}$  of the average transverse momentum of charged particles versus baryochemical potential  $\mu_B$  for the 7.2 % most central  $Pb+Pb$  collisions (full symbols, NA49 [21]) and inelastic  $p+p$  interactions (open symbols, NA61/SHINE preliminary [107]). Expectations for a critical point assuming correlation lengths of  $\xi = 3$  (6) fm are shown by full (dashed) curves. Results are for cms rapidity  $1.1 < y < 2.6$  calculated assuming the pion mass.

For the same reactions preliminary results have also become available for the fluctuation quantities  $\Delta[X, N]$  and  $\Sigma[X, N]$  introduced in Sec. IIIB, where  $X$  is the sum of absolute transverse momenta of the  $N$  particles in the acceptance region of the analysis. Figure 13

displays the results from Ref. [107]. Note that  $\Phi_{p_T}$  is related to  $\Sigma[X, N]$  by Eq. (33) and for the IPM one expects for these quantities the values of 0 and 1 respectively. The quantity  $\Delta[X, N]$  is sensitive to fluctuations of  $X$  and  $N$  differently than  $\Sigma[X, N]$ . Both measures show results which are close to the IPM expectations and display no distinct features in their energy dependence.

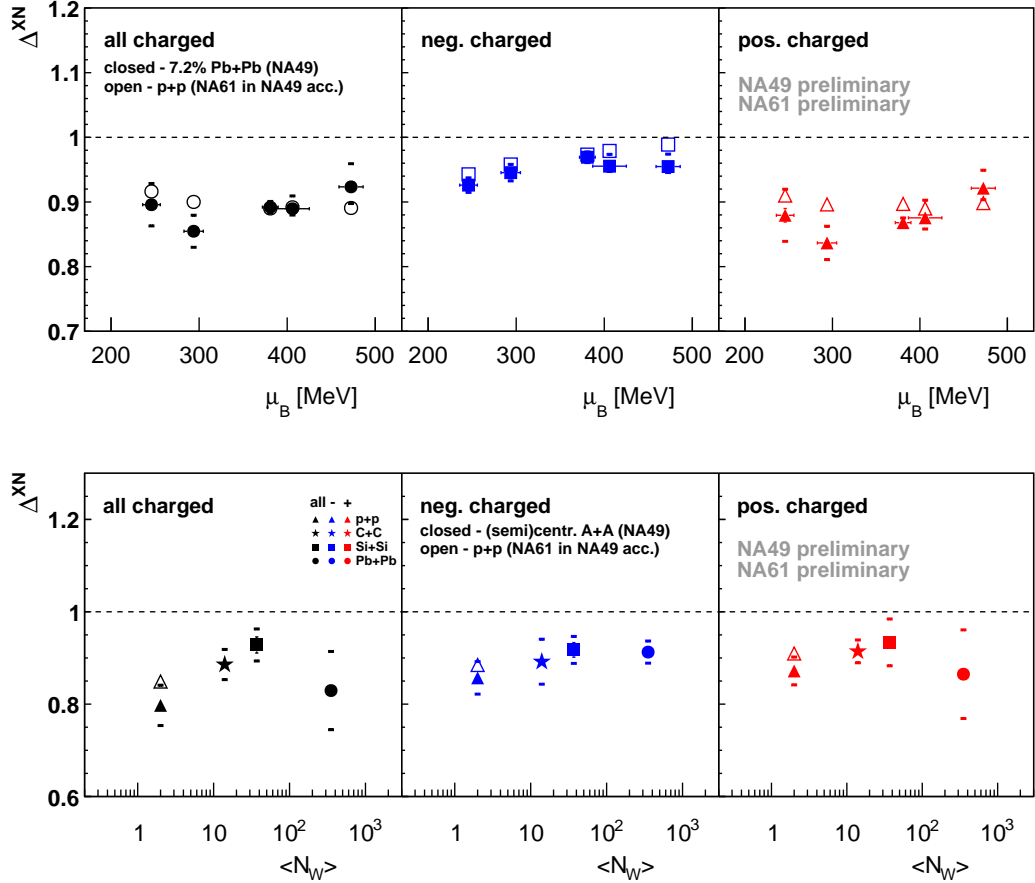


Figure 13: Fluctuation measures  $\Sigma[X, N]$  (top) and  $\Delta[X, N]$  (bottom) of the sum of transverse momenta  $X$  of charged particles versus  $\mu_B$  for the 7.2 % most central Pb+Pb collisions (full symbols) and inelastic p+p interactions (open symbols). Results are for cms rapidity  $1.1 < y < 2.6$  assuming the pion mass (NA49 and NA61/SHINE preliminary [107]).

### C. Fluctuation Studies with Incomplete Particle Identification

Fluctuations of the chemical (particle-type) composition of hadronic final states in A+A collisions are expected to be sensitive to the phase transition between hadronic and partonic matter. First experimental results on e-by-e chemical fluctuations have already been published from the CERN SPS and BNL RHIC, and more systematic measurements are in progress. The e-by-e fluctuations of hadron multiplicities have been studied theoretically in statistical models (see, e.g. Ref. [108–111]) and in dynamical transport models (see, e.g. review [112] and references therein).

Studies of chemical fluctuations in general require to determine the number of particles of different hadron species (e.g. pions, kaons, and protons) e-by-e. A serious experimental problem in such measurements is incomplete particle identification, i.e. the impossibility to identify uniquely the type of each detected particle. The effect of particle mis-identification distorts the measured fluctuation quantities. For this reason the analysis of chemical fluctuations is usually performed in a small acceptance, where particle identification is relatively reliable. However, an important part of the information on e-by-e fluctuations in full phase space is then lost.

Although it is usually impossible to identify each detected particle, one can nevertheless determine with high accuracy the average multiplicities (averaged over many events) for different hadron species.

#### 1. The Identity Method

In Ref. [113] a new experimental technique called the *identity method* was proposed. It solved the misidentification problem for one specific combination of the second moments in a system of two hadron species (‘kaons’ and ‘pions’). In Refs. [114, 115] this method was extended to show that all the second moments as well as the higher moments of the joint multiplicity distribution of particles of different types can be uniquely reconstructed in spite of the effects of incomplete identification. Notably, the identity method can be used for an arbitrary number  $k \geq 2$  of hadron species. Following Ref. [113] we assume that particle identification is achieved by measuring the particle mass  $m$ . Since any measurement is of finite resolution, we deal with continuous distributions of observed masses denoted as  $\rho_j(m)$  and normalized as ( $j = 1, \dots, k \geq$



2)

$$\int dm \rho_j(m) = \langle N_j \rangle . \quad (53)$$

Note that for experimental data the functions  $\rho_j(m)$  for particles of type  $j$  are obtained from the inclusive distribution of the  $m$ -values for all particles from all collision events. The identity variables  $w_j(m)$  are defined as

$$w_j(m) \equiv \frac{\rho_j(m)}{\rho(m)} , \quad \rho(m) \equiv \sum_{i=1}^k \rho_i(m) . \quad (54)$$

Complete identification (CI) of particles corresponds to distributions  $\rho_j(m)$  which do not overlap. In this case,  $w_j = 0$  for all particle species  $i \neq j$  and  $w_j = 1$  for the  $j$ th species. When the distributions  $\rho_j(m)$  overlap,  $w_j(m)$  can take the value of any real number from  $[0, 1]$ . We introduce the quantities

$$W_j \equiv \sum_{i=1}^{N(n)} w_j(m_i) , \quad W_j^2 \equiv \left( \sum_{i=1}^{N(n)} w_j(m_i) \right)^2 , \quad W_p W_q \equiv \left( \sum_{i=1}^{N(n)} w_p(m_i) \right) \times \left( \sum_{i=1}^{N(n)} w_q(m_i) \right) , \quad (55)$$

with  $j = 1, \dots, k$  and  $1 \leq p < q \leq k$ , and define their event averages as

$$\langle W_j^2 \rangle = \frac{1}{N_{\text{ev}}} \sum_{n=1}^{N_{\text{ev}}} W_j^2 , \quad \langle W_p W_q \rangle = \frac{1}{N_{\text{ev}}} \sum_{n=1}^{N_{\text{ev}}} W_p W_q , \quad (56)$$

where  $N_{\text{ev}}$  is the number of events, and  $N(n) = N_1(n) + \dots + N_k(n)$  is the total multiplicity in the  $n$ th event. Each experimental event is characterized by a set of particle masses  $\{m_1, m_2, \dots, m_N\}$ , for which one can calculate the full set of identity variables:  $\{w_j(m_1), w_j(m_2), \dots, w_j(m_N)\}$ , with  $j = 1, \dots, k$ . Thus, the quantities  $W_j$ ,  $W_j^2$ , and  $W_p W_q$  are completely defined for each event, and their average values (56) can be found experimentally by straightforward e-by-e averaging. The main idea is to find the relations between these  $W$ -quantities and the unknown moments of the multiplicity distribution  $\langle N_j^2 \rangle$  and  $\langle N_p N_q \rangle$ . In the case of CI, one finds  $W_j = N_j$ , thus, Eq. (56) yields

$$\langle W_j^2 \rangle = \langle N_j^2 \rangle , \quad \langle W_p W_q \rangle = \langle N_p N_q \rangle . \quad (57)$$

The quantities  $\langle W_j^2 \rangle$  and  $\langle W_q W_p \rangle$  can be calculated as follows

$$\begin{aligned}
\langle W_j^2 \rangle &= \sum_{N_1=0}^{\infty} \sum_{N_2=0}^{\infty} \dots \sum_{N_k=0}^{\infty} \mathcal{P}(N_1, \dots, N_k) \int dm_1^1 P_1(m_1^1) \dots \int dm_{N_1}^1 P_1(m_{N_1}^1) \\
&\times \int dm_1^2 P_2(m_1^2) \dots \int dm_{N_2}^2 P_2(m_{N_2}^2) \times \dots \times \int dm_1^k P_k(m_1^k) \dots \int dm_{N_k}^k P_k(m_{N_k}^k) \\
&\times \left[ w_j(m_1^1) + \dots w_j(m_{N_1}^1) + w_j(m_1^2) + \dots + w_j(m_{N_2}^2) + \dots + w_j(m_1^k) + \dots + w_j(m_{N_k}^k) \right]^2 \\
&= \sum_{i=1}^k \langle N_i \rangle [u_{ji}^2 - (u_{ji})^2] + \sum_{i=1}^k \langle N_i^2 \rangle (u_{ji})^2 + 2 \sum_{1 \leq i < l \leq k} \langle N_i N_l \rangle u_{ji} u_{jl} , \tag{58}
\end{aligned}$$

$$\begin{aligned}
\langle W_p W_q \rangle &= \sum_{N_1=0}^{\infty} \sum_{N_2=0}^{\infty} \dots \sum_{N_k=0}^{\infty} \mathcal{P}(N_1, \dots, N_k) \int dm_1^1 P_1(m_1^1) \dots \int dm_{N_1}^1 P_1(m_{N_1}^1) \\
&\times \int dm_1^2 P_2(m_1^2) \dots \int dm_{N_2}^2 P_2(m_{N_2}^2) \times \dots \times \int dm_1^k P_k(m_1^k) \dots \int dm_{N_k}^k P_k(m_{N_k}^k) \\
&\times \left[ w_p(m_1^1) + \dots w_p(m_{N_1}^1) + w_p(m_1^2) + \dots + w_p(m_{N_2}^2) + \dots + w_p(m_1^k) + \dots + w_p(m_{N_k}^k) \right] \\
&\times \left[ w_q(m_1^1) + \dots w_q(m_{N_1}^1) + w_q(m_1^2) + \dots + w_q(m_{N_2}^2) + \dots + w_q(m_1^k) + \dots + w_q(m_{N_k}^k) \right] \\
&= \sum_{i=1}^k \langle N_i \rangle [u_{pqi} - u_{pi} u_{qi}] + \sum_{i=1}^k \langle N_i^2 \rangle u_{pi} u_{qi} + \sum_{1 \leq i < l \leq k} \langle N_i N_l \rangle [u_{pi} u_{ql} + u_{pl} u_{qi}] . \tag{59}
\end{aligned}$$

In Eqs. (58) and (59),  $\mathcal{P}(N_1, \dots, N_k)$  is the multiplicity distribution,  $P_i(m) \equiv \rho_i(m)/\langle N_i \rangle$  are the mass probability distributions of the  $i$ th species, and ( $s = 1, 2$ )

$$u_{ji}^s \equiv \frac{1}{\langle N_i \rangle} \int dm w_j^s(m) \rho_i(m) , \quad u_{pqi} \equiv \frac{1}{\langle N_i \rangle} \int dm w_p(m) w_q(m) \rho_i(m) . \tag{60}$$

In the case of CI, when the distributions  $\rho_j(m)$  do not overlap, one finds that

$$u_{ji}^s = \delta_{ji} , \quad u_{pqi} = 0 , \tag{61}$$

and Eqs. (58) and (59) reduce then to Eq. (57). The incomplete particle identification transforms the second moments  $\langle N_j^2 \rangle$  and  $\langle N_p N_q \rangle$  to the quantities  $\langle W_j^2 \rangle$  and  $\langle W_p W_q \rangle$ , respectively. Each of the later quantities contains linear combinations of all the first and second moments,  $\langle N_i \rangle$  and  $\langle N_i^2 \rangle$ , as well as all the correlation terms  $\langle N_i N_l \rangle$ . Having introduced the notations

$$\langle W_j^2 \rangle - \sum_{i=1}^k \langle N_i \rangle [u_{ji}^2 - (u_{ji})^2] \equiv b_j , \quad \langle W_p W_q \rangle - \sum_{i=1}^k \langle N_i \rangle [u_{pqi} - u_{pi} u_{qi}] \equiv b_{pq} , \tag{62}$$

one can transform Eqs. (58) and (59) to the following form:

$$\sum_{i=1}^k \langle N_i^2 \rangle u_{ji}^2 + 2 \sum_{1 \leq i < l \leq k} \langle N_i N_l \rangle u_{ji} u_{jl} = b_j, \quad j = 1, 2, \dots, k, \quad (63)$$

$$\sum_{i=1}^k \langle N_i^2 \rangle u_{pi} u_{qi} + \sum_{1 \leq i < l \leq k} \langle N_i N_l \rangle (u_{pi} u_{ql} + u_{pl} u_{qi}) = b_{pq}, \quad 1 \leq p < q \leq k. \quad (64)$$

The right-hand side of Eqs. (63) and (64) defined by Eq. (62) are experimentally measurable quantities. The same is true for the coefficients  $u_{ji}^s$  (with  $s = 1$  and  $2$ ) entering the left-hand side of Eqs. (63) and (64). Therefore, Eqs. (63) and (64) represent a system of  $k + k(k-1)/2$  linear equations for the  $k$  second moments  $\langle N_j^2 \rangle$  with  $j = 1, \dots, k$  and  $k(k-1)/2$  correlators  $\langle N_p N_q \rangle$  with  $1 \leq p < q \leq k$ . In order to solve Eqs. (63) and (64) we introduce the  $[k + k(k-1)/2] \times [k + k(k-1)/2]$  matrix  $A$

$$A = \left( \begin{array}{ccc|ccc} a_1^1 & \dots & a_1^k & a_1^{12} & \dots & a_1^{(k-1)k} \\ \cdot & \cdot & \cdot & \cdot & \cdot & \cdot \\ \cdot & \cdot & \cdot & \cdot & \cdot & \cdot \\ a_k^1 & \dots & a_k^k & a_k^{12} & \dots & a_k^{(k-1)k} \\ \hline a_{12}^1 & \dots & a_{12}^k & a_{12}^{12} & \dots & a_{12}^{(k-1)k} \\ \cdot & \cdot & \cdot & \cdot & \cdot & \cdot \\ \cdot & \cdot & \cdot & \cdot & \cdot & \cdot \\ a_{12}^k & \dots & a_{(k-1)k}^k & a_{(k-1)k}^{12} & \dots & a_{(k-1)k}^{(k-1)k} \end{array} \right), \quad (65)$$

where

$$a_j^i \equiv u_{ji}^2, \quad 1 \leq i, j \leq k; \quad a_i^{pq} \equiv 2u_{ip}u_{iq}, \quad 1 \leq p < q \leq k, \quad i = 1, \dots, k; \quad (66)$$

$$a_{pq}^i \equiv u_{pi}u_{qi}, \quad 1 \leq p < q \leq k, \quad i = 1, \dots, k; \quad (67)$$

$$a_{pq}^{lm} \equiv u_{pl}u_{qm} + u_{ql}u_{pm}, \quad 1 \leq p < q \leq k, \quad 1 \leq l < m \leq k. \quad (68)$$

The solution of Eqs. (63) and (64) can be presented by Cramer's formulas in terms of the determinants

$$\langle N_j^2 \rangle = \frac{\det A_j}{\det A}, \quad \langle N_p N_q \rangle = \frac{\det A_{pq}}{\det A}, \quad (69)$$

where the matrices  $A_j$  and  $A_{pq}$  are obtained by substituting in the matrix  $A$  the column  $a_1^j, \dots, a_k^j, a_{12}^j, \dots, a_{(k-1)k}^j$  and the column  $a_1^{pq}, \dots, a_k^{pq}, a_{12}^{pq}, \dots, a_{(k-1)k}^{pq}$ , respectively, for the column  $b_1, \dots, b_k, b_{12}, \dots, b_{(k-1)k}$ . Therefore, if  $\det A \neq 0$ , the system of linear equations (63) and (64) has a unique solution (69) for all the second moments. In the case of CI (61), one finds  $\det A = 1$ ,  $\det A_j = b_j$ , and  $\det A_{pq} = b_{pq}$ . The solution (69) reduces then to Eq. (57).

Introducing the  $[k + k(k-1)/2]$ -vectors

$$\mathcal{N} \equiv \begin{pmatrix} \langle N_1^2 \rangle \\ \dots \\ \langle N_k^2 \rangle \\ \langle N_1 N_2 \rangle \\ \dots \\ \langle N_{k-1} N_k \rangle \end{pmatrix}, \quad \mathcal{B} \equiv \begin{pmatrix} b_1 \\ \dots \\ b_k \\ b_{12} \\ \dots \\ b_{(k-1)k} \end{pmatrix}, \quad (70)$$

one can write Eqs. (63) and (64) in the matrix form  $A\mathcal{N} = \mathcal{B}$ . The solution (69) can be then rewritten as

$$\mathcal{N} = A^{-1} \mathcal{B}, \quad (71)$$

where  $A^{-1}$  is the inverse matrix of  $A$ . For two particle species,  $k = 2$ , this solution takes the form

$$\begin{pmatrix} \langle N_1^2 \rangle \\ \langle N_2^2 \rangle \\ \langle N_1 N_2 \rangle \end{pmatrix} = \begin{pmatrix} u_{11}^2 & u_{12}^2 & 2u_{11}u_{12} \\ u_{21}^2 & u_{22}^2 & 2u_{21}u_{22} \\ u_{11}u_{21} & u_{12}u_{22} & u_{11}u_{22} + u_{12}u_{21} \end{pmatrix}^{-1} \begin{pmatrix} b_1 \\ b_2 \\ b_{12} \end{pmatrix}. \quad (72)$$

Then Eq. (72) yields

$$\langle N_1^2 \rangle = \frac{b_1 u_{22}^2 + b_2 u_{12}^2 - 2b_{12} u_{12} u_{22}}{(u_{11} u_{22} - u_{12} u_{21})^2}, \quad (73)$$

$$\langle N_2^2 \rangle = \frac{b_2 u_{11}^2 + b_1 u_{21}^2 - 2b_{12} u_{21} u_{11}}{(u_{11} u_{22} - u_{12} u_{21})^2}, \quad (74)$$

$$\langle N_1 N_2 \rangle = \frac{b_{12}(u_{11} u_{22} + u_{12} u_{21}) - b_1 u_{22} u_{21} - b_2 u_{11} u_{12}}{(u_{11} u_{22} - u_{12} u_{21})^2}. \quad (75)$$

The above procedure eliminates the effect of misidentification and provides the values of all the second moments  $\langle N_j^2 \rangle$  and  $\langle N_p N_q \rangle$  in a model-independent way, as they would be obtained

in an experiment in which each particle is uniquely identified. Recently the identity method was generalized to determine third and higher moments of the multiplicity distributions in events consisting of an arbitrary number of different particle species [115]. As emphasized in Refs. [60, 61], measurements of the third and higher moments of event-by-event fluctuations are, in fact, expected to be more sensitive for the search of the critical point in nucleus-nucleus collisions.

## 2. First Results on Fluctuations Based on the Identity Method

Experiments NA49 and NA61/SHINE identify particles by measuring their ionisation energy loss  $dE/dx$  in the TPC tracking chambers. From a typical inclusive distribution of the obtained  $dE/dx$  values, as shown in Fig. 14, it is evident that the contributions of protons, kaons, pions and electrons overlap. For measuring the fluctuations of their numbers one can try to fit the  $dE/dx$  distributions event-by-event as was done by NA49 previously [20, 22]. However, this method has serious statistical limitations and can only be applied to high-multiplicity events such as produced in Pb+Pb collisions. To overcome this problem and be able to study multiplicity fluctuations for the full range of nuclei from p to Pb the NA49 and NA61/SHINE collaborations are now employing the identity method.

The distributions  $\rho_j(m \equiv dE/dx)$  of Eq. (53) are determined from precise fits to the inclusive distributions of  $dE/dx$  (see curves in Fig. 14 as an example). Using the  $\rho_j$  one then derives the distributions of identities  $w_j(m \equiv dE/dx)$  of Eq. (54) (see Fig. 15, left) which correspond to the probabilities for a particle with  $m = dE/dx$  to be of type  $j$ . The analogue  $W_j$  of the multiplicity distribution of particles of type  $j$ , calculated according to Eqs. (55, 56) (see Fig. 15, right), is continuous for incomplete particle identification. Moreover the multiplicities of particles of types  $j$  and  $k$  are in general correlated. One obtains from Eq. (56) the pure and mixed second moments of the smeared multiplicity distributions from which the moments of the true multiplicity distributions are found by the matrix inversion procedure of the identity method [114].

The moments corrected for the effects of incomplete particle identification can then be used to compute the scaled variance  $\omega$  of the multiplicity distributions of  $p+\bar{p}$ ,  $K^+ + K^-$  and  $\pi^+ + \pi^-$ . The results for inelastic p+p interactions and the 3.5 % most central Pb+Pb collisions plotted

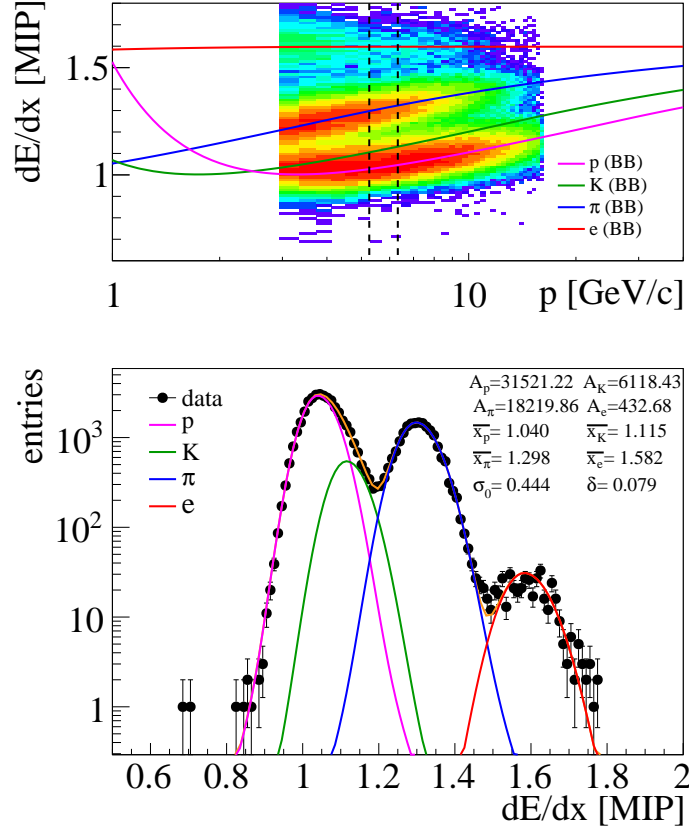


Figure 14:  $dE/dx$  distributions for Pb+Pb collisions at 20.4 GeV from NA49 [116]. Upper panel: Measured  $dE/dx$  values as function of reconstructed momenta for the phase space region  $0.4 < p_\perp$  [GeV/c]  $< 0.6$  and  $135 < \phi$  [°]  $< 180$ . Lines correspond to calculations with the Bethe-Bloch (BB) formula for different particle types. Lower panel: Projection of the upper plot onto the vertical axis in the momentum interval  $5.2 < p$  [GeV/c]  $< 6.4$  indicated by vertical dashed lines. Colored lines represent the  $dE/dx$  distribution functions of different particles.

versus the collision energy  $\sqrt{s_{NN}}$  are shown in Fig. 16 (see Ref. [107]). One observes no peak structure which might be attributed to the effects of a critical point. A similar conclusion was reached for  $\omega$  of unidentified charged particles in Ref. [25]. The stronger increase of  $\omega$  for pions seen in Fig. 16 is mostly due to the more relaxed centrality selection for Pb+Pb collisions and the fact that the scaled variance is only an intensive and not a strongly intensive quantity.

As the identity method allows to determine all pure and mixed first and second moments

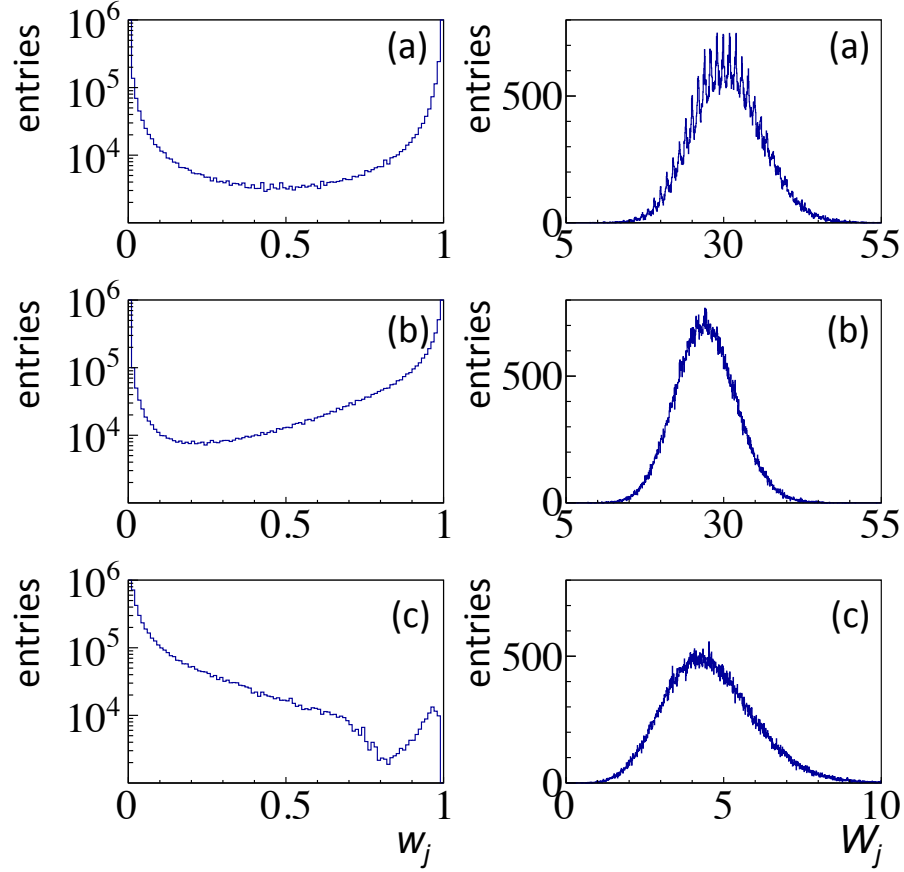


Figure 15: Left panel: Distributions of  $w_j$  of Eq. (54) for (a) pions, (b) protons and (c) kaons for central Pb+Pb collisions at 20A GeV. Right panel: Corresponding distributions of  $W_j$  of Eq. (55) [116].

of the multiplicity distributions of  $p+\bar{p}$ ,  $K^+ + K^-$  and  $\pi^+ + \pi^-$ , one is able to derive the values of the strongly intensive quantity  $\Phi[A, B]$  defined in Eq. (34).  $\Phi[A, B]$  measures fluctuations between particle types, so-called chemical fluctuations. The results for the three possible pair combinations are displayed in Fig. 17 for inelastic p+p interactions from NA61/SHINE and central Pb+Pb collisions from NA49 (see Ref. [117]). The values of  $\Phi$  are close to that resulting from the IPM, i.e. the the fluctuations are mostly statistical. However, one observes some systematic energy dependence and changes of sign, the origin of which need to be understood.

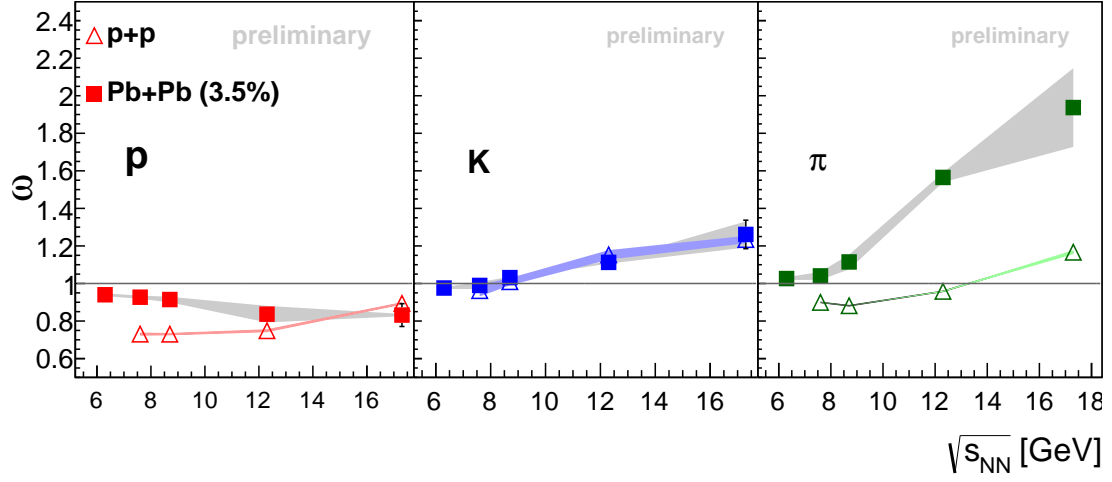


Figure 16: Scaled variance  $\omega$  of the multiplicity distributions of  $p+\bar{p}$ ,  $K^+ + K^-$  and  $\pi^+ + \pi^-$  in inelastic p+p and the 3.5 % most central Pb+Pb collisions versus the collision energy  $\sqrt{s_{NN}}$  [107].

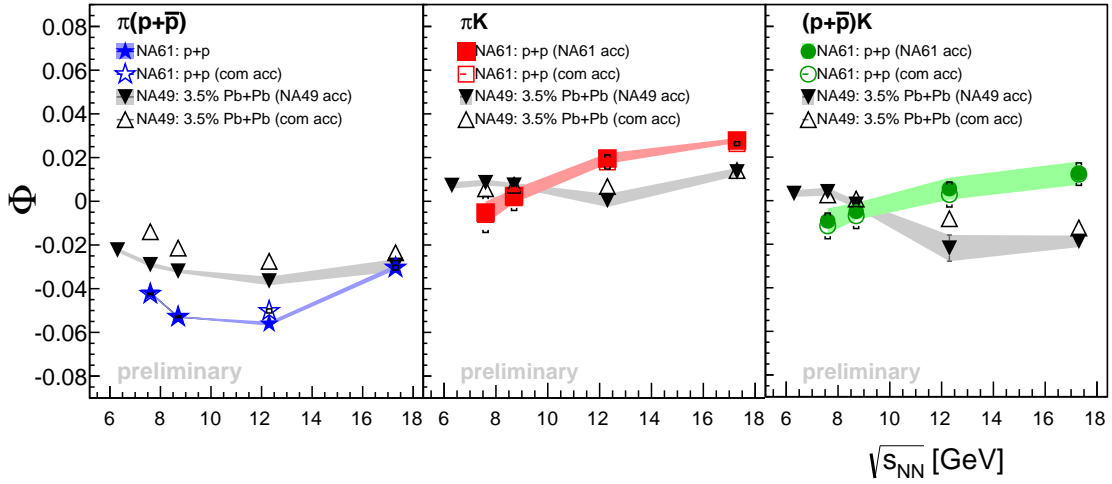


Figure 17: Strongly intensive fluctuation quantity  $\Phi$  measured for identified particle pairs in inelastic p+p and the 3.5 % most central Pb+Pb collisions versus collision energy  $\sqrt{s_{NN}}$  [117].



#### IV. CLOSING REMARKS

Experimental study of strongly interacting matter started in the 1970s with experiments at JINR Dubna and LBL Berkeley recording first collisions of relativistic heavy ions. Since then rich experimental data on Pb+Pb and Au+Au collisions were collected at energies ranging from several GeV to several TeV. Single particle spectra and mean multiplicities were precisely measured in fixed target experiments, whereas the most comprehensive results on correlations in azimuthal angle of hadrons produced at mid-rapidity were obtained in collider experiments.

These results clearly indicate that a system of strongly interacting particles created in heavy ion collisions at high energies is close to, at least, local equilibrium. At freeze-out the system occupies a volume which is much larger than a volume of individual hadron. The latter conclusion is based on the failure of dynamical and the success of statistical [118] and hydrodynamical models [119]. Thus, one concludes that strongly interacting matter is created in heavy ion collisions.

The phase transition of strongly interacting matter to the QGP - the onset of deconfinement - was discovered with the energy scan program of NA49 at the CERN SPS [9, 10]. The program was motivated by the predictions of the statistical model of the early stage of collisions. The discovery is based on the observation that several basic hadron production properties measured in heavy ion collisions rapidly change their dependence on collision energy in a common energy domain [11].

The experimental discoveries of strongly interacting matter and the onset of deconfinement ask for further studies, in particular systematic results on event-by-event fluctuations are still missing. The fluctuations are difficult to measure as one cannot correct for the limited acceptance of detectors using forward-backward and rotational symmetries. Here large acceptance detectors are needed. Moreover, precise control is required over fluctuations of the number of nucleons which participate in the collisions. The measurement of strongly intensive quantities will further mitigate the effects of remaining participant number fluctuations.

These challenges are currently addressed by NA61/SHINE at the CERN SPS and STAR BES II at the BNL RHIC with the help of significant upgrades of the legacy detectors. Furthermore, the methods to study event-by-event fluctuations have recently advanced significantly. All this should lead to new data on event-by-event fluctuations which will soon shed more light on

properties of the onset of deconfinement and will have potential for the discovery of the critical point.

The third generation experiments, MPD at JINR NICA and CBM at FAIR SIS, are originally planned to use multi-purpose detectors. They are mostly optimized for high statistics measurements of low cross-section processes. Thus new future experiments dedicated to measurements of event-by-event fluctuations are needed. Their detectors should measure almost all charged hadrons with a low background and allow for a precise determination of the number of spectator nucleons ideally from both colliding nuclei. The highest event rate is not the top priority in the study of bulk properties of strongly interacting matter via analysis of event-by-event fluctuations.

### Acknowledgements

This work was supported by the National Science Centre of Poland (grant UMO-2012/04/M/ST2/00816), the German Research Foundation (grants GA 1480/2-1, GA 1480/2-2), and the State Agency of Science, Innovations and Informatization of Ukraine (contract F58/384-2013).

- 
- [1] M. Stephanov, PoS LAT2006, **24** (2006).
  - [2] F. Becattini *et al.*, Phys. Rev. **C69**, 024905 (2004); **C73**, 044905 (2006).
  - [3] J. Cleymans *et al.*, Phys. Rev. **C73**, 034905 (2006).
  - [4] U. W. Heinz and M. Jacob, arXiv:nucl-th/0002042.
  - [5] J. Rafelski and B. Müller, Phys. Rev. Lett. **48**, 1066 (1982) [Erratum-ibid. **56**, 2334 (1986)].
  - [6] T. Matsui and H. Satz, Phys. Lett. B **178**, 416 (1986).
  - [7] F. Becattini, L. Maiani, F. Piccinini, A. D. Polosa and V. Riquer, Phys. Lett. B **632**, 233 (2006).
  - [8] M. Gazdzicki and M. I. Gorenstein, Acta Phys. Polon. **B30**, 2705 (1999).
  - [9] C. Alt *et al.* [NA49 Collaboration], Phys. Rev. C **77**, 024903 (2008).
  - [10] S. V. Afanasiev *et al.* [NA49 Collaboration], Phys. Rev. C **66**, 054902 (2002).
  - [11] M. Gazdzicki, M. Gorenstein, P. Seyboth, Acta Phys. Polon. **B42**, 307 (2011).

- [12] M. Gazdzicki and D. Röhrich, Z. Phys. **C65**, 215 (1995).
- [13] M. Gazdzicki and D. Röhrich, Z. Phys. **C71**, 55 (1996).
- [14] E. Fermi, Prog. Theor. Phys. **5**, 570 (1950).
- [15] L. D. Landau, Izv. Akad. Nauk SSSR Ser. Fiz. **17**, 51 (1953).
- [16] M. Gazdzicki, Proceedings of NATO Advanced Research Workshop: "Hot Hadronic Matter: Theory and Experiment", Divonne-les-Bains, France, June 27 – July 1 (1994), edited by J. Letessier, H. H. Gutbrod and J. Rafelski, NATO ASI Series B: Physics Vol. 346, Plenum Press (1995) 215.
- [17] M. Gazdzicki, Z. Phys. **C66**, 659 (1995).
- [18] M. Gazdzicki, J. Phys. G23, 1881 (1997).
- [19] J. Bächler *et al.* [NA49 Collaboration], *Searching for QCD Phase Transition*, Addendum–1 to Proposal SPSLC/P264, CERN/SPSC 97 (1997).
- [20] T. Anticic *et al.* [NA49 Collaboration], Phys. Rev. C **83**, 061902 (2011).
- [21] T. Anticic *et al.* [NA49 Collaboration], Phys. Rev. C **79**, 044904 (2009).
- [22] C. Alt *et al.* [NA49 Collaboration], Phys. Rev. C **79**, 044910 (2009).
- [23] C. Alt *et al.* [NA49 Collaboration], Phys. Rev. C **78**, 044907 (2008).
- [24] C. Alt *et al.* [NA49 Collaboration], Phys. Rev. C **78**, 034918 (2008).
- [25] C. Alt *et al.* [NA49 Collaboration], Phys. Rev. C **78**, 034914 (2008).
- [26] C. Alt *et al.* [NA49 Collaboration], Phys. Rev. C **77**, 064908 (2008).
- [27] C. Alt *et al.* [NA49 Collaboration], Phys. Rev. C **76**, 024914 (2007).
- [28] C. Alt *et al.* [NA49 Collaboration], Phys. Rev. C **73**, 044910 (2006).
- [29] T. Anticic *et al.* [NA49 Collaboration], Phys. Rev. C **69**, 024902 (2004).
- [30] L. Van Hove, Phys. Lett. **B118**, 138 (1982).
- [31] C. Hung and E. Shuryak, Phys. Rev. Lett. **75**, 4003 (1995).
- [32] J. Cleymans and K. Redlich, Phys. Rev. C **60**, 054908 (1999).
- [33] H. Sorge, H. Stöcker and W. Greiner, Nucl. Phys. A **498**, (1989) 567C.
- [34] S. A. Bass *et al.*, Prog. Part. Nucl. Phys. **41**, 225 (1998).
- [35] W. Cassing and E.L. Bratkovskaya, Phys. Rep. **308**, 65 (1999).
- [36] W. Cassing, E. L. Bratkovskaya, and S. Juchem, Nucl. Phys. A **674**, 249 (2000).

- [37] M. I. Gorenstein, M. Gazdzicki and K. A. Bugaev, Phys. Lett. B **567**, 175 (2003).
- [38] M. Gazdzicki, M. I. Gorenstein, F. Grassi, Y. Hama, T. Kodama and O. J. Socolowski, Braz. J. Phys. **34**, 322 (2004).
- [39] Y. Hama, F. Grassi, O. Socolowski, T. Kodama, M. Gazdzicki and M. Gorenstein, Acta Phys. Polon. B **35**, 179 (2004).
- [40] H. G. Fischer, slides from the open 74th Meeting of the SPSC, November 15, 2005, <http://indico.cern.ch/conferenceDisplay.py?confId=a057199>.
- [41] B. A. Cole *et al.*, Phys. Lett. B **639**, 210 (2006).
- [42] A. Bialas and W. Czyz, Acta Phys. Polon. B **36**, 905 (2005).
- [43] M. Gazdzicki and M.I. Gorenstein, Phys. Lett. B **640**, 155 (2006).
- [44] H. Bialkowska, M. Gazdzicki, W. Retyk and E. Skrzypczak, Z. Phys. C **55**, 491 (1992).
- [45] M. Gazdzicki *et al.* [NA61/SHINE Proto-Collaboration], *A New Experimental Programme with Nuclei and Proton Beams at the CERN SPS*, CERN-SPSC-2003-038; SPSC-EOI-001
- [46] M. Gazdzicki, M. I. Gorenstein and S. Mrowczynski, Phys. Lett. B **585**, 115 (2004).
- [47] M. I. Gorenstein, M. Gazdzicki and O. S. Zozulya, Phys. Lett. B **585**, 237 (2004).
- [48] J.-Y. Ollitrault, Phys. Rev. D **46**, 229 (1992).
- [49] P. F. Kolb, J. Sollfrank and U. W. Heinz, Phys. Rev. C **62**, 054909 (2000).
- [50] N. Antoniou *et al.* [NA61/SHINE Collaboration], *Study of the hadron production in hadron-nucleus and nucleus-nucleus collisions at CERN SPS*, CERN-SPSC-2006-034.
- [51] N. Abgrall *et al.* [NA61 Collaboration], arXiv:1401.4699 [physics.ins-det].
- [52] N. Abgrall *et al.* [NA61 Collaboration], CERN-SPSC-2013-028; SPSC-SR-124.
- [53] F. Arleo *et al.* [CHIC Proto-Collaboration], CERN-SPSC-2012-031; SPSC-EOI-008.
- [54] G. S. F. Stephans, J. Phys. G **32**, S447 (2006).
- [55] G. Odyniec, PoS CPOD **2013**, 043 (2013).
- [56] White paper [STAR Collaboration]: *Studying the Phase Diagram of QCD Matter at RHIC*, <https://drupal.star.bnl.gov/STAR/starnotes/public/sn0598> (2014).
- [57] L. Adamczyk *et al.* [STAR Collaboration], Phys. Rev. C **88**, 014902 (2013).
- [58] E. Sangaline [STAR Collaboration], Nucl. Phys. A, **904-905**, 771c (2013).
- [59] Y. Hatta and M. Stephanov, Phys. Rev. Lett. **91**, 102003 (2003).

- [60] M.A. Stephanov, Phys. Rev. Lett. **107**, 052301 (2011).
- [61] M.A. Stephanov, Phys. Rev. Lett. **102**, 032301 (2009).
- [62] C. Athanasiou, K. Rajagopal, and M. Stephanov, Phys. Rev. D **82**, 074008 (2010).
- [63] L. Adamczyk *et al.* [STAR Collaboration], Phys. Rev. Lett. **112**, 032302 (2014).
- [64] A. Rustamov, <https://indico.cern.ch/conferenceDisplay.py?confId=144745>
- [65] L. Kumar [STAR Collaboration], J. Phys. G **38**, 124145 (2011).
- [66] B. Mohanty [STAR Collaboration], J. Phys. G **38**, 124023 (2011).
- [67] J. Schukraft *et al.* [ALICE Collaboration ], J. Phys. G **38**, 124003 (2011).
- [68] A. Toia *et al.* [ALICE Collaboration ], J. Phys. G **38**, 124007 (2011).
- [69] J. P. Lansberg, V. Chambert, J. P. Didelez, B. Genolini, C. Hadjidakis, P. Rosier, R. Arnaldi and E. Scomparin *et al.*, PoS QNP **2012**, 049 (2012).
- [70] K. .U. Abraamyan, S. V. Afanasiev, V. S. Alfeev, N. Anfimov, D. Arkhipkin, P. Z. .Aslanyan, V. A. Babkin and M. I. Baznat *et al.*, Nucl. Instrum. Meth. A **628**, 99 (2011).
- [71] P. Senger [CBM Collaboration], Cent. Eur. J. Phys., **10**, 1289 (2012); see also <http://www.fair-center.eu/for-users/experiments/cbm.html>.
- [72] A. N. Sissakian *et al.* [NICA Collaboration], J. Phys. G **36**, 064069 (2009).
- [73] NICA White Paper, January 24, 2014, [http://theor.jinr.ru/twiki/pub/NICA/WebHome/WhitePaper\\_10.01.pdf](http://theor.jinr.ru/twiki/pub/NICA/WebHome/WhitePaper_10.01.pdf)
- [74] see <http://www.fair-center.eu/public.html>.
- [75] J. Randrup and J. Cleymans, Phys. Rev. C **74**, 047901 (2006).
- [76] V. Koch, in *Relativistic Heavy Ion Physics*, Landold-Börnstein Volume I/23, edited by R. Stock (Springer, Berlin, 2010).
- [77] I. N. Mishustin, Phys. Rev. Lett. **82**, 4779 (1999); Nucl. Phys. A **681**, 56c (2001).
- [78] H. Heiselberg and A. D. Jackson, Phys. Rev. C **63**, 064904 (2001).
- [79] M. Stephanov, K. Rajagopal, and E. Shuryak, Phys. Rev. Lett. **81**, 4816 (1998).
- [80] M. Stephanov, K. Rajagopal, and E. Shuryak, Phys. Rev. D **60**, 114028 (1999).
- [81] M. Stephanov, Acta Phys. Polon. B **35**, 2939 (2004).
- [82] V. Koch, A. Majumder and J. Randrup, Phys. Rev. Lett. **95**, 182301 (2005).
- [83] V. Koch, A. Majumder and J. Randrup, Phys. Rev. C **72**, 064903 (2005).

- [84] W. Broniowski and W. Florkowski, Phys. Rev. C **65**, 024905 (2002).
- [85] V.P. Konchakovski, M. Hauer, G. Torrieri, M.I. Gorenstein, and E.L. Bratovskaya, Phys. Rev. C **79**, 034910 (2009).
- [86] V. P. Konchakovski, B. Lungwitz, M. I. Gorenstein, and E. L. Bratkovskaya, Phys. Rev. C **70**, 024906 (2008).
- [87] A. Bialas, M. Bleszynski, and W. Czyz, Nucl. Phys. B **111**, 461 (1976).
- [88] V. P. Konchakovski, S. Haussler, M. I. Gorenstein, E. L. Bratkovskaya, M. Bleicher, and H. Stöcker, Phys. Rev. C **73**, 034902 (2006).
- [89] F. Becattini, J. Manninen, and M. Gazdzicki, Phys. Rev. C **73**, 044905 (2006).
- [90] M. Gazdzicki [NA61/SHINE Collaboration], J. Phys. G **36**, 064039 (2009).
- [91] G. Odyniec [STAR Collaboration], J. Phys. G **35**, 104164 (2008);
- [92] M. I. Gorenstein and M. Gazdzicki, Phys. Rev. C **84**, 014904 (2011).
- [93] M. Gazdzicki, M. I. Gorenstein, and M. Mackowiak-Pawłowska, Phys. Rev. C **88**, 024907 (2013).
- [94] M. Gazdzicki, Eur. Phys. J. C **8**, 131 (1999).
- [95] M. Gaździcki and St. Mrowczyński, Z. Phys. C **54**, 127 (1992).
- [96] M. I. Gorenstein, J. Phys. G **35**, 125102 (2008).
- [97] V. V. Begun, M. Gazdzicki and M. I. Gorenstein, Phys. Rev. C **78**, 024904 (2008).
- [98] S. V. Afanasev *et al.* [NA49 Collaboration], Phys. Rev. Lett. **86**, 1965 (2001).
- [99] N. Antoniou *et al.* [NA61/SHINE Collaboration], CERN-SPSC-2006-034.
- [100] V. V. Begun, V. P. Konchakovski, M. I. Gorenstein and E. Bratkovskaya, J. Phys. G **40**, 045109 (2013).
- [101] M. I. Gorenstein and M. Rybczynski, Phys. Lett. B **730**, 70 (2014).
- [102] K. Grebieszkow, Acta Phys. Polon. B **43**, 1333 (2012).
- [103] M. I. Gorenstein and K. Grebieszkow, Phys. Rev. C **89**, 034903 (2014).
- [104] M. Stephanov, private communication.
- [105] K. Grebieszkow [NA49 Collaboration], Nucl. Phys. A **830**, 547c (2009).
- [106] Z. Fodor and S. Katz, JHEP **04**, 50 (2004).
- [107] P. Seyboth [NA49 and NA61/SHINE Collaborations], Proceedings Contribution arXiv:1402.4619; see also slides at <https://atlaswww.hep.anl.gov/ismd13/>.

- [108] V. V. Begun, M. Gazdzicki, M. I. Gorenstein, and O. S. Zozulya, Phys. Rev. C **70**, 034901 (2004).
- [109] V.V. Begun, M.I. Gorenstein, M. Hauer, V.P. Konchakovski, and O.S. Zozulya, Phys. Rev. C **74**, 044903 (2006).
- [110] V.V. Begun, M. Gazdzicki, M.I. Gorenstein, M. Hauer, V.P. Konchakovski, and B. Lungwitz, Phys. Rev. C **76**, 024902 (2007).
- [111] M. I. Gorenstein and M. Hauer, Phys. Rev. C **78**, 041902 (2008).
- [112] V.P. Konchakovski, M.I. Gorenstein, E.L. Bratkovskaya, and W. Greiner, J. Phys. G **37**, 073101 (2010).
- [113] M. Gazdzicki, K. Grebieszko, M. Maćkowiak, and S. Mrówczyński, Phys. Rev. C **83**, 054907 (2011).
- [114] M. I. Gorenstein, Phys. Rev. C **84**, 024902 (2011).
- [115] A. Rustamov and M.I. Gorenstein, Phys. Rev. C **86**, 044906 (2012).
- [116] T. Anticic *et al.* [NA49 Collaboration], arXiv:1310.3428 (2013).
- [117] M. Mackowiak-Pawłowska [NA49 and NA61/SHINE Collaborations], PoS (CPOD 2013), 048.
- [118] F. Becattini, arXiv:0901.3643 [hep-ph].
- [119] W. Florkowski, *Phenomenology of Ultra-Relativistic Heavy-Ion Collisions* World Scientific, ISBN: 9814280666, 436 pages, 2010.